UNIVERSITY OF PARDUBICE

FACULTY OF CHEMICAL TECHNOLOGY

DOCTORAL THESIS

2025 Jakub Halamek

University of Pardubice

Faculty of Chemical Technology

Adsorptive Separation of Small Molecules on Zeolitic Materials

Jakub Halamek

Doctoral Thesis

2025

I hereby declare:

I have independently authored the thesis entitled “Adsorptive Separation of Small Molecules on Zeolitic Materials”. All literary sources and information used in the thesis are listed in the bibliography.

I am aware that my thesis is subject to the rights and obligations arising from Act No. 121/2000 Coll., on copyright, on rights related to copyright, and on amendments to certain laws (Copyright Act), as amended, in particular the fact that the University of Pardubice has the right to enter into a license agreement for the use of this work as a school work pursuant to Section 60(1) of the Copyright Act, and that if I use this work myself or grant a license for its use to another entity, the University of Pardubice is entitled to request a reasonable contribution from me to cover the costs incurred in creating the work, up to the full amount of such costs, depending on the circumstances.

I acknowledge that, in accordance with Section 47b of Act No. 111/1998 Coll., on Higher Education Institutions and on Amendments and Supplements to Other Acts (the Higher Education Act), as amended, and the University of Pardubice Directive No. 7/2019 Rules for Submission, Publication, and Formatting of Final Theses, as amended, the thesis will be published through the Digital Library of the University of Pardubice.

In Pardubice, 30th June 2025.

Jakub Halamek

ACKNOWLEDGEMENT

First and foremost, I would like to thank my supervisor, prof. Roman Bulánek, for his scientific guidance, patience, and financial support over the course of my doctoral studies. I would also like to thank my co-workers Eva Pozdílková, Ph.D., Kateřina Knotková, Ph.D., and Dr. Safaa Essid for their help in the laboratory, as well as our collaborators, Dr. Ota Bludský, Miroslav Rubeš, Ph.D., and Ing. Tomáš Volný, for their contribution to the research presented in this work.

Lastly, I would like to thank my parents, my brother, and my sisters, for their support and their patience with me throughout these years.

ABSTRACT

This doctoral thesis investigates various phenomena influencing the capacity of zeolite structures to perform the adsorptive separation of CO_2/CH_4 and light hydrocarbon (C_2 – C_4) mixtures, two of the most important contemporary research problems in the development of adsorptive separation processes. A large variety of zeolite materials is investigated within the scope of this thesis - particularly those possessing the chabazite (**CHA)** and Linde type-A (**LTA**) framework, as well as a set of materials recently synthesized by the so-called ADOR process from the **UTL** and **UOV** precursors. More specifically, this doctoral thesis aims to gain deeper insights into the influence of the chemical composition of the zeolite framework, the nature and quantity of the charge-compensating extra-framework cations, and the zeolite framework topology (influencing the pore size and shape), on the adsorption of CO_2 and light hydrocarbons in well selected zeolite systems, as well as to explain hitherto unexplained adsorption phenomena, observed in some specific zeolites, related to the presence of structural imperfections in the zeolite structure. The presented research was carried out using a combination of quantitative experiments, performed on volumetric and gravimetric devices, designed to investigate both the adsorption equilibria and kinetics, coupled with advanced characterization methods (adsorption microcalorimetry, in-situ FTIR employing probe molecules, MAS NMR, PXRD) and computational methods (performed by the collaborators - Dr. Ota Bludský et al.).

KEYWORDS

zeolite, adsorption, separation, carbon dioxide, hydrocarbon, extra-framework cation

ANOTACE

Tato disertační práce se zabývá různými jevy ovlivňujícími schopnost zeolitových struktur provádět adsorpční separaci směsí CO_2/CH_4 a lehkých uhlovodíků (C_2 – C_4), v současnosti jedny z dvou nejdůležitějších výzkumných problémů v oblasti vývoje adsorpčních separačních procesů. V rámci této práce je zkoumána široká škála zeolitových materiálů – zejména materiály na bázi chabazitové (**CHA**) a **LTA** mřížky, a také soubor materiálů nedávno syntetizovaných tzv. ADOR procesem z **UTL**, resp. **UOV** prekurzorů. Konkrétním cílem této disertační práce je získání hlubšího vhledu do vlivu chemického složení zeolitové mřížky, charakteru a množství mimomřížkových kationtů a topologie mřížky (ovlivňující velikost a tvar pórů) na adsorpci CO_2 a lehkých uhlovodíků ve specificky vybraných zeolitových systémech, a dále vysvětlit dosud neobjasněné adsorpční chování některých specifických systémů, související s přítomností strukturních nedokonalostí ve struktuře zeolitu. Prezentovaný výzkum byl proveden na základě kombinace kvantitativních experimentů, prováděných na volumetrických a gravimetrických aparaturách, určených ke zkoumání adsorpčních rovnováh i kinetiky, ve spojení s pokročilými charakterizačními metodami (adsorpční mikrokalorimetrie, in-situ FTIR s využitím zkušebních molekul, MAS NMR, PXRD) a výpočetními metodami (provedenými spolupracovníky – Dr. Otou Bludským a kol.).

KLÍČOVÁ SLOVA

zeolit, adsorpce, separace, oxid uhličitý, uhlovodík, mimomřížkový kationt

LIST OF PAPERS

This doctoral thesis is written in the form of a commented set of scientific papers. The publications presented here were composed in the years 2021 – 2025 at the Department of Physical Chemistry, Faculty of Chemical Technology, University of Pardubice, mostly in collaboration with the Institute of Organic Chemistry and Biochemistry (IOCB) of the Czech Academy of Sciences.

I) Qiudi Yue, Jakub Halamek, Daniel N. Rainer, Jin Zhang, Roman Bulánek, Russell E. Morris, Jiří Čejka, Maksym Opanasenko
Tuning the CHA framework composition by isomorphous substitution for CO_2/CH_4 separation.
Chemical Engineering Journal, 429, 2022, 131277. DOI: 10.1016/j.cej.2021.131277.

II) Michal Trachta, Tomáš Volný, Roman Bulánek, Eva Koudelková, Jakub Halamek, Miroslav Rubeš, Mariya Shamzhy, Michal Mazur, Jiří Čejka, Ota Bludský
Strong CO_2 adsorption in narrow-pore ADOR zeolites: A combined experimental and computational study on IPC-12 and related structures.
Journal of CO_2 Utilization, 74, 2023, 102548. DOI: 10.1016/j.jcou.2023.102548.

III) Jakub Halamek, Roman Bulánek, Miroslav Rubeš, Ota Bludský
Properties of multiple Lewis acid sites in alkali metal-exchanged chabazites probed by CO adsorption.
Microporous and Mesoporous Materials, 374, 2024, 113152. DOI: 10.1016/j.micromeso.2024.113152.

IV) Jakub Halamek, Martin Kubů, Branislav Koreň, Jiří Čejka, Roman Bulánek, Jan Valenta
Selective CO_2 adsorption over alkali metal cation-exchanged UZM-9 zeolites.
Submitted manuscript (Journal of CO_2 Utilization).

V) Jakub Halamek, Tomáš Volný, Roman Bulánek, Jan Blahut, Jiří Čejka, Pavla Eliášová, Maksym Opanasenko, Ota Bludský
Defect-controlled adsorptive separation of propane and propene on the PCR zeolite synthesized by the ADOR process.
Finalized manuscript.

TRAINEESHIPS

- School of Catalysis 2021, prof. Jiří Čejka; Liblice Castle, Czech Republic; 4 – 6th October 2021.
- Summer School and Workshop in Calorimetry and Thermal Analysis 2022, National Centre for Scientific Research (CNRS), Dr. Aline Auroux; Lyon, France; 19 – 24th June 2022.
- School on Adsorption 2023, Charles University, Faculty of Science, Department of Physical and Macromolecular Chemistry, prof. Jiří Čejka; Prague, Czech Republic; 7 – 8th February 2023.
- Workshop on Textural Characterization of Porous Materials, Czech Academy of Sciences, Institute of Chemical Process Fundamentals, Dr. Martin A. Thomas; Prague, Czech Republic; 20th April 2023.
- The 4th School of X-ray microanalysis, Czech Academy of Sciences, Institute of Physics, Mgr. Karel Jurek, prof. Ondřej Gedeon; Prague, Czech Republic; 3 – 5th October 2023.
- **School of Chemistry, University of St Andrews, prof. Russell E. Morris; St Andrews, United Kingdom; 15th January – 15th April 2024.**
- School of Catalysis 2024, prof. Jiří Čejka; Liblice Castle, Czech Republic; 28 – 30th May 2024.

ORAL AND POSTER PRESENTATIONS

The results obtained throughout my doctoral studies have been presented in the following oral presentations:

- Jakub Halamek, Roman Bulánek, Safaa Essid, Adsorption of small molecules in CHA zeolites, Workshop on Zeolites, Liblice Castle, Czech Republic, 24 – 27th October 2021.
- Jakub Halamek, Roman Bulánek, Safaa Essid, Effect of differing Si/Al on the adsorption and separation of CH_4/CO_2 over Na-CHA zeolites, 5th International Conference on Applied Surface Science, Palma de Mallorca, Spain, 25 – 28th April 2022.

- Jakub Halamek, Roman Bulánek, Eva Koudelková, Michal Trachta, Adsorptive separation of C_4 hydrocarbons using the IPC-4 zeolite synthesized by the ADOR process, School on Catalysis 2023, Liblice Castle, Czech Republic, 23 – 25th May 2023.

- Jakub Halamek, Roman Bulánek, Kateřina Knotková, The synthesis and application of boron-heterosubstituted AlPO zeotypes, Workshop on Tailoring Reaction Pathways by Catalysis, Liblice Castle, Czech Republic, 3 – 6th September 2023.

And in the following poster presentations:

- Jakub Halamek, Roman Bulánek, Adsorption properties of stacked 1D chain Mn-dhbq coordination polymer, Workshop on Low-Dimensional Materials, Liblice Castle, Czech Republic, 19 – 22nd September 2022.

- Jakub Halamek, Roman Bulánek, Miroslav Rubeš, Ota Bludský, The influence of extra-framework (EF) alkali-metal cations on the adsorption of CO on CHA zeolite framework, NanoCAT Summer School 2024, J. Heyrovský Institute of Physical Chemistry, Prague, Czech Republic, 22 – 24th July 2024.

TABLE OF CONTENTS

1. INTRODUCTION

Gas mixtures consisting of compounds with small molecules such as air, natural gas, various flue gases, light hydrocarbon mixtures, etc., are of key importance in many industrial applications. Very often, it is, however, necessary to modify the composition of the available gas feed to make it suitable for the given application. This may entail the removal of an undesired impurity (for example H_2S or CO_2) or, in some other cases, a bulk separation of the original feed into several new fractions (in order to isolate desired compounds from the mixture, for example). In industry, small molecule gas mixtures are traditionally separated either by processes based on fractional distillation or on gas absorption in a solution (scrubbing). Both of these types of processes are generally very energy-intensive.

In the case of distillation, it is usually necessary to work at high pressures (up to several hundred atm) and sometimes very low temperatures as it is impossible to perform the liquefaction of a gas at a higher temperature than its critical temperature (which for example in the case of nitrogen and oxygen is 126.2 and 154.6 K respectively[1, 2]). In addition to the above, if the boiling points of the components we wish to separate are similar, very high reflux ratios and distillation columns with large numbers of trays are required to obtain fractions of desired purities. An example of a particularly energy-intensive distillation-based process is the separation of propane and propene. In the case of the industrial synthesis of propene by propane dehydrogenation, the distillation of this mixture was reported to account for about 85 % cost of the entire process[3].

Gas absorption-based processes are usually employed for the removal of acid gas impurities such as CO_2 or H_2S (for example from natural gas). Systems for gas absorption generally consist of two main parts, the absorption column and the regeneration column. The main absorption column operates at a high pressure (up to a hundred atm) and usually contains a water solution of an organic base (e.g., an amine) that can bind the acid molecules present in the feed. The regeneration of the amine absorbent is then performed by boiling the water solution in the regeneration column, which incurs significant energy costs. In addition to the high energy cost, the amine absorbents used in the process can pose health and environmental hazards. For these reasons, alternative less energy-intensive approaches are required in order to lower the gas separation costs.

Broadly speaking, there exist two such approaches, membrane separations and adsorptive separations. Both types of processes are already used with great success in many industrial

applications such as air separation, hydrogen separation from heavier gases and drying of various gas mixtures. In the case of membrane separations, the feed under higher pressure (commonly about 10 atm) is pushed into a cartridge containing a membrane, which is permeated at a different rate by each component of the feed, causing the desired separation effect. Adsorption-based separation processes utilize materials with very high specific surface area (adsorbents) tailored specifically so that they interact differently with different components of the gas mixture. Several different molecular-scale mechanisms accounting for the resulting separation effect have been reported – they will be discussed in Section 2.

Industrial adsorption separations are generally performed in continuous cyclical processes using two (or more) parallel adsorbent-filled columns. At any given time, the gas feed always flows through only one column, where some of its components are adsorbed, while others remain in the gas leaving the column (fraction 1). At the same time, the second column is getting regenerated after being saturated in the previous step, releasing the adsorbed components in the process (fraction 2). When the saturation of the first column and the regeneration of the second column are finished, the gas flow is sent through the freshly regenerated column while the saturated column undergoes regeneration and the cycle continues. Depending on how the regeneration is performed there are three general setups used in industry: (1) pressure swing adsorption (PSA), where adsorption is generally performed at elevated pressures (5-10 atm), while regeneration is performed mostly at the atmospheric pressure, (2) vacuum swing adsorption (VSA), where adsorption is generally performed at atmospheric or slightly elevated pressures (up to 2 atm), while regeneration requires sub-atmospheric pressures and (3) temperature swing adsorption (TSA), where the regeneration is not performed by the change in pressure, but by heating the regenerated column, usually not higher than to 373 K. In addition to these three basic processes, a combined PTSA procedure, performing the regeneration by simultaneous changes in both pressure and temperature, has also been developed[4].

As both the membrane- and adsorption-based processes are generally operated at room temperature and the regeneration is either not needed or doesn't require the heating of large quantities of liquid water, the costs are usually significantly smaller than in the case of the more traditional approaches described above. It should be noted, however, that achieving required purities may be exceedingly difficult, which is the main reason why, for some applications, the significantly more energy-intensive distillation or absorption processes continue to be used.

2. ADSORPTION

According to IUPAC, adsorption is defined as an increase in the concentration of a dissolved substance at the interface of a condensed and a liquid phase (or alternatively at the interface of a condensed and a gas phase) due to the operation of surface forces[5]. The condensed phase is usually called *adsorbent*, while the molecules of the dissolved substance are either called *adsorptive* (if they're free in the liquid/gas phase) or *adsorbate* (if they're present at the interface of the liquid/gas phase and the condensed phase). Since the subject of this thesis is the adsorption of small gas molecules on solids, the following text will only consider gas-solid interfaces.

The most commonly used macroscopic quantitative characteristic of a gas-solid adsorption equilibrium is usually the *adsorption isotherm* (Eq. 1) – a dependence of the quantity q_a of an adsorbing compound a in the interface (usually expressed as the molar amount, mass, or volume) on its quantity in the gas phase (usually expressed as pressure p) at constant temperature.

$$q_a = f(p)_{T=const.} \tag{1}$$

An explicit expression for a general adsorption isotherm in a single-gas component system (Gibbs adsorption isotherm) can be derived from the theory of thermodynamics of phase boundaries (Eq. 2)

$$\Gamma_a = -\left(\frac{\partial \gamma}{\partial \mu_a}\right)_T = -\frac{1}{RT}\left(\frac{\partial \gamma}{\partial \ln f_a}\right)_T = -\frac{f_a}{RT}\left(\frac{\partial \gamma}{\partial f_a}\right)_T \tag{2}$$

where Γ_a is the surface adsorption of the adsorbate a (in mol/m^2), γ is the surface tension on the interface, μ_a is the chemical potential of a, and f_a is the fugacity of a. This expression is, however, not very practical since the quantities it relates are generally impossible to obtain experimentally, and for this reason, different adsorption models are generally used to describe the experimental data, such as the mechanistically derived Langmuir (Eq. 3) (for single-layer adsorption) and BET models (for multi-layer adsorption) or semi-empirical models like the Tóth isotherm (Eq. 4).

$$q_a = \frac{q_m b p}{1 + bp} \tag{3}$$

$$q_a = \frac{q_m b p}{[(1 + bp)^t]^{1/t}} \tag{4}$$

where q_a is the amount of adsorbate a (usually in mol, mL or g per 1 g of adsorbent), b is the equilibrium constant of adsorption and t is a non-ideality constant.

From the perspective of the molecular scale, a gas molecule can interact with a surface by weak interactions or by a chemical bond. If chemical bonds do arise, the process is called chemisorption. As the energy of a chemical bond is significantly larger (usually in the magnitude of hundreds of kJ/mol), one can generally neglect the relatively small contributions of weak interactions (in the scale of dozens of kJ/mol). Chemisorption takes place only on specific active sites on the adsorbent surface, is often highly selective to some adsorbate molecules, and usually results in the formation of stable chemical bonds that cannot be easily broken by a change in pressure. The site specificity of chemisorption implies a relatively low uptake capacity of the adsorbent, which, along with the potential elevated costs of regeneration (if the process is reversible at all), makes this mechanism usually unsuitable for gas separations. If, however, only weak chemical bonds are formed and hence the regeneration costs are in an acceptable range (regeneration by a pressure swing is possible), chemisorption can be harnessed for a highly selective removal of an impurity that is present in small amounts in the initial gas feed or even for bulk separations. The most important applications of chemisorption-based gas separation processes in industry are based on the formation of weak chemical bonds between active sites on the surface and π-electrons of the adsorbate (also called π-complexation). Such interactions are highly selective to compounds with double-bonds while being relatively easy to break. The most important commercial application of π-complexation-based separations as is the CO bulk separation/recovery from syngas (using CuCl/alumina or CuCl/activated carbon adsorbents)[6, 7].

If no chemical bonds are generated during the interaction, the process is called physisorption. It should be pointed out that physisorption-based separation processes account for the majority of adsorption-based separation processes operated commercially. The physisorption interaction energy is generally given by a sum of two different effects – the adsorbent-adsorbate interaction and adsorbate-adsorbate (lateral) interaction. The adsorbate-adsorbate interaction can usually be adequately approximated by the condensation energy of the adsorptive. As such, this effect thermodynamically favors the adsorption of species characterized by stronger cohesive forces, such as species that contain hydrogen bonds when in the liquid phase or gases in subcritical state as opposed to supercritical state. This effect is negligible at low uptakes and only manifests itself as the pores start to be filled with the adsorbate.

The decisive factor in adsorption is usually, however, the adsorbent-adsorbate interaction. Several different effects contribute to the overall interaction energy between a linear gas molecule and a surface in the case of physisorption (Eq. 5)[7]:

$$\phi = \phi_D + \phi_R + \phi_{Ind} + \phi_{F\mu} + \phi_{\dot{F}Q} \tag{5}$$

where ϕ is the total adsorbate-adsorbent interaction energy, ϕ_D is the dispersion energy, ϕ_R is the close-range repulsion energy, ϕ_{Ind} is the energy of interaction between an electric field and an induced dipole, $\phi_{F\mu}$ is the energy of interaction between an electric field and a permanent dipole and $\phi_{\dot{F}Q}$ is the energy of interaction between an electric field gradient and a quadrupole (note that the interaction between an electric field and a quadrupole is always zero). The functional forms for these contributions are in Eq. 6-10.[7]

$$\phi_D = -\frac{A}{r^6} \tag{6}$$

$$\phi_R = \frac{B}{r^{12}} \tag{7}$$

$$\phi_{Ind} = -\frac{1}{2}\alpha F^2 = -\frac{1}{2}\alpha\left(\frac{1}{4\pi\varepsilon_0}\frac{q}{r^2}\right)^2 = -\frac{\alpha q^2}{32\pi^2\varepsilon_0^2 r^4} \tag{8}$$

$$\phi_{F\mu} = -F\mu\cos\theta = -\frac{1}{4\pi\varepsilon_0}\frac{q}{r^2}\mu\cos\theta = -\frac{q\mu\cos\theta}{4\pi\varepsilon_0 r^2} \tag{9}$$

$$\phi_{\dot{F}Q} = \frac{1}{2}Q\dot{F} = -\frac{Qq(3\cos^2\theta - 1)}{4r^3(4\pi\varepsilon_0)} \tag{10}$$

where r is the distance between the interacting atoms (of adsorbent and adsorbate), A is a constant defined by the Kirkwood-Müller formula (Eq. 11) and B is another constant related to A (by the Eq. 12), α is the polarizability of the adsorbate, F is the electric field of a surface atom, ε_0 is the vacuum permittivity, q is the electric charge on a surface atom, μ is the permanent dipole moment of the adsorbate, θ is the angle between the direction of the field or the field gradient and the axis of the dipole or linear quadrupole and Q is the linear quadrupole moment of the adsorbate.

$$A = \frac{6mc^2\alpha_1\alpha_2}{\frac{\alpha_1}{\chi_1} + \frac{\alpha_2}{\chi_2}} \tag{11}$$

$$B = \frac{Ar_0^6}{2} \tag{12}$$

In these two expressions, m is the mass of the electron, c is the speed of light, α_1 and α_2 are the polarizabilities of the interacting atoms, χ_1 and χ_2 are their magnetic susceptibilities and r_0 is the mean of the Van der Waals radii of both atoms.

ϕ_D and ϕ_R are non-specific and present in all adsorbate-adsorbent systems and together form the so-called Lennard-Jones potential. The remaining contributions depend on both the nature of the adsorbent surface and the nature of the adsorbate molecule. If an adsorbent has a nonpolar surface (e.g. an activated carbon), it generates no electrical field and thus ϕ_{Ind}, $\phi_{F\mu}$ and $\phi_{\dot{F}Q}$ are zero. The overall adsorbate-adsorbent interaction can then be expressed in eq. 13 as follows.

$$\phi = \phi_D + \phi_R = A(\alpha) \cdot \left(-\frac{1}{r^6} + \frac{r_0^6}{2r^{12}} \right) \tag{13}$$

As A is nearly proportional (see Eq. 11) to the polarizability α of the adsorbate, so is the total adsorption potential ϕ. More polarizable molecules (those with larger and more dispersed electron clouds) will therefore exhibit larger affinity for the adsorbent, while molecules with less electrons will interact less intensively with the same adsorbent. This fact can be leveraged, for example, for selective removal of organic impurities (VOC) such as solvents from air or vent streams (for example with the help of the abovementioned activated carbon).

In the case of an adsorbent boasting a polar surface (e.g. a metal oxide, a zeolite, silica, alumina or a metal-organic framework – MOF) ϕ_{Ind}, $\phi_{F\mu}$ and $\phi_{\dot{F}Q}$ are usually the decisive contributions, although still of similar magnitude to the non-specific contributions ϕ_D and ϕ_R, which can therefore not be neglected. The contribution of ϕ_{Ind} (Eq. 8) depends on the strength of the electric field F generated by the adsorbent surface (which depends on the distance from the surface) and on the polarizability α of the adsorbate molecule. As such, similarly to the dispersion forces, molecules with larger and more dispersed electron clouds will be able to acquire a larger dipole moment and will thus interact more strongly with a polar surface, increasing the already present preference due to non-specific interactions.

$\phi_{F\mu}$ (Eq. 9) represents the classical electrostatic interaction given by the strength of the electric field generated by the surface (which again depends on the distance from the surface), by the permanent dipole moment of the adsorbate, and by the orientation of the dipole towards the field. As a result of this contribution to the overall interaction, polar adsorbates such as H_2O or CO have a stronger affinity to a polar surface than nonpolar adsorbates such as CH_4 or O_2. This mechanism is the basis for some of the most important industrially operated adsorption-based separation processes, such as drying of various gas-feeds (air, natural gas, syngas, hydrocarbon

streams), hydrogen purification (removal of CO, CH_4, CO_2), or desulfurization of hydrocarbon streams. Various zeolite-, silica-, or alumina-based adsorbents are commonly used in these applications[7].

Finally, the contribution of $\phi_{\dot{F}Q}$ (Eq. 10) depends on the size of the gradient of the electric field generated by the adsorbent surface and on the quadrupole moment of the adsorbate molecule. In order for this contribution to be significant, it is necessary that an adsorbent have an irregular distribution of electric charge on its surface. This is satisfied, for example, in the case of zeolites containing extra-framework cations compensating the negative charge of the framework. Such an adsorbent can then exhibit significantly increased preference for molecules with large quadrupole moments, even if they possess small polarizability and no dipole moment (such as CO_2 or N_2). The most important industrial applications of this mechanism are the air separation and CO_2 removal from hydrocarbon streams, both of which employ zeolites as adsorbents[7].

Separation mechanisms based on differences in adsorbate-adsorbent interaction described above are based on thermodynamic properties of the system in equilibrium and they assume that the adsorbent surface is fully accessible to all molecules of the gas mixture. In real systems, however, the accessibility of adsorbent surface can vary considerably for different gas molecules, in particular with relation to the size and shape of their molecules.

If an adsorbent possesses a regular porous structure where the pore diameters are comparable to the kinetic diameters of molecules in the gas mixture, for example, widely different diffusion rates may be observed for different molecules, a fact that can be leveraged in the so-called "kinetics-based" separation, despite a possible lack of major differences in equilibrium behavior. This mechanism isn't commonly employed on its own as it is difficult to obtain adsorbents with pore sizes and sufficiently narrow pore distributions appropriate for specific applications, but it is usually used in conjunction with equilibrium-governed mechanisms to enhance the effectiveness of the process. The only major commercial application based primarily on the difference in diffusivities of the gas molecules in the pores of an adsorbent is the air separation using carbon molecular sieves (CMS) (in the PSA setup). CO_2 separation from CH_4 and N_2 and light olefin/paraffin separations using CMS, MOFs or high/pure-silica zeolites are also considered[7, 8].

If the diffusion rate for some compounds is so small that their molecules are effectively excluded from the pore system (or a part thereof), we're talking about the so-called "molecular-sieving effect". This mechanism usually results in the exclusion of some larger molecules

present in the gas mixture from entering the pore system, allowing to perform gas separations with very high selectivity. In order for this effect to be employed, it is usually necessary to use crystalline adsorbents such as zeolites or MOFs, as an extremely narrow pore-size distribution, which is impossible to obtain otherwise, is required for the molecular-sieving effect to work.

In the case of zeolites, one specific way to enhance or even bring about the molecular-sieving effect is to exploit the presence of extra-framework cations attached to their crystalline framework, namely by engineering zeolitic materials where the extra-framework cations of a specific type and in sufficient quantity are localized in or around the pore openings, reducing the accessibility of the pores for some guest-species (resulting in the so-called "gate" effect). The two most important commercial applications of molecular sieving are drying of various gases and the separation of linear paraffins from iso-paraffins and cyclic hydrocarbons. Both of these applications employ zeolite A as the adsorbent, in each case modified to an appropriate extra-framework cation form to achieve maximum selectivity utilizing the abovementioned gate effect.

The two mechanisms described above (kinetics-based separation and molecular sieving) assume that the adsorbent has an inflexible, rigid structure. This is usually an acceptable approximation, for some systems, however, it cannot be applied. This is especially true for the as-of-yet industrially unapplied metal-organic frameworks (MOFs), some of which exhibit extremely flexible crystalline frameworks. The extent to which a flexible framework is "open" or "closed" generally depends on the physical conditions of the system (temperature and pressure) as well as on the presence and nature of adsorbate gas. In the literature on MOFs, systems were reported where adsorption led to a decrease in pore volume ("pore breathing")[9] as well as systems where it led to an increase in pore volume ("pore swelling")[10]. Interestingly enough, the phenomenon of "pore breathing" was also observed for some zeolites such as ITQ-55 during the adsorption of ethene[11]. Lab-scale experiments have shown that both "pore breathing" and "pore swelling" could be exploited for highly selective gas separations[9, 10]. As of yet, however, no commercial application exists.

Other than the flexibility of the framework, the flexibility of extra-framework cation position in zeolites has also been observed. In particular, for low-silica zeolites containing extra-framework cations in the pore openings (and therefore capable of "gate effect"-based molecular sieving), it was shown that depending on physical conditions of the system (temperature and pressure), some adsorbate molecules that should be excluded due to their kinetic diameter are

able deviate the extra-framework cation from its equilibrium position to the extent that they can then diffuse inside the pore system, while other molecules are unable to get past the cation. This can effectively result in "size-inverse molecular sieving" if the excluded molecules have a smaller kinetic diameter than the molecules that manage to penetrate inside the pore system. This mechanism has been called the "molecular trapdoor" effect and has primarily been used to perform a highly selective adsorption of CO_2 over CH_4 and N_2 on low silica potassium-, rubidium- or cesium-exchanged chabazite zeolites[12]. As of now, this process has been tested on a laboratory pilot-plant scale[13].

3. ZEOLITES

Zeolites are inorganic crystalline materials that were first discovered and characterized by the Swedish mineralogist and chemist Axel Fredrik Cronstedt in the mid. 18th century[14] to whom they also owe their name, composed of Ancient Greek words ζεῖν [zeín] meaning "to boil/to heat/to bubble up" and λίθος [líthos] meaning "a stone", yielding a neologism ζεόλιθος [zeólithos], which literally means "a boiling stone". This name refers to their characteristic behavior observed by Cronstedt, namely the evolution of large quantities of water vapor upon heating of the raw mineral (in his case stilbite). This behavior is related to several of the characteristic properties of zeolites, summarized by the following up-to-date definition by the International Mineralogical Association (IMA)[15]:

"A zeolite mineral is a crystalline substance with a structure characterized by a framework of linked tetrahedra, each consisting of four O atoms surrounding a cation. This framework contains open cavities in the form of channels and cages. These are usually occupied by H_2O molecules and extra-framework cations that are commonly exchangeable. The channels are large enough to allow the passage of guest species. In the hydrated phases, dehydration occurs at temperatures mostly below about 673 K and is largely reversible. The framework may be interrupted by (OH, F) groups; these occupy a tetrahedron apex that is not shared with adjacent tetrahedra."

Generally speaking, the definition above allows for materials with a wide range of chemical compositions. Historically, however, zeolites were primarily thought of as aluminosilicate minerals, which is still generally the case as these are utilized in the vast majority of real-life zeolite applications. As of now, various zeolitic frameworks have been synthesized in the form of aluminosilicate, pure-silica (zeosils), aluminophosphate (AlPO), silico-aluminophosphate (SAPO), germanosilicate and other materials – each chemical composition providing the material with a unique set of physico-chemical properties. It should be pointed out that some sources reserve the term "zeolite" only for the aluminosilicates, preferring to place materials of different chemical composition under the term "zeotypes". This doctoral thesis will be employing the term "zeolite" in its broader sense, in line with the up-to-date IMA definition.

Exact description of the chemical composition using a chemical formula can be done in various ways – detailed discussion and recommendations have been provided by the International Union of Pure and Applied Chemistry (IUPAC) and International Zeolite Association (IZA)[16]. Usually, however, a simple formula of the form $[M_{\frac{x}{n}}(H_2O)_p][Al_xSi_yO_{2(x+y)}]$, or alternatively

$M_{\frac{x'}{n}}O_{\frac{x'}{2}} \cdot x'Al_2O_3 \cdot y'SiO_2 \cdot pH_2O$, suffices (assuming an aluminosilicate zeolite with a single type of extra-framework cation). In these formulae M^{n+} is the extra-framework cation with the charge n, p is the level of hydration of the zeolite and x and y are stoichiometric coefficients (or x' and y' – in this case $x' = x/2$, $y' = y$) providing a key characteristic of the zeolite, namely its $Si/Al = y/x = y'/2x'$ ratio (with a limitation that $Si/Al > 1$ – the so-called Löwenstein rule[17]). The importance of this parameter stems from the fact that, as is clear from the two formulae, the amount of framework aluminum is directly tied to the quantity of extra-framework cations – this is due to the fact that aluminum atoms bring negative charge to the framework that subsequently requires the presence of an appropriate quantity of extra-framework cations for charge compensation. A simple illustration of an elementary structural motive of a zeolite framework is in Fig. 1 (taken from the literature[18]).

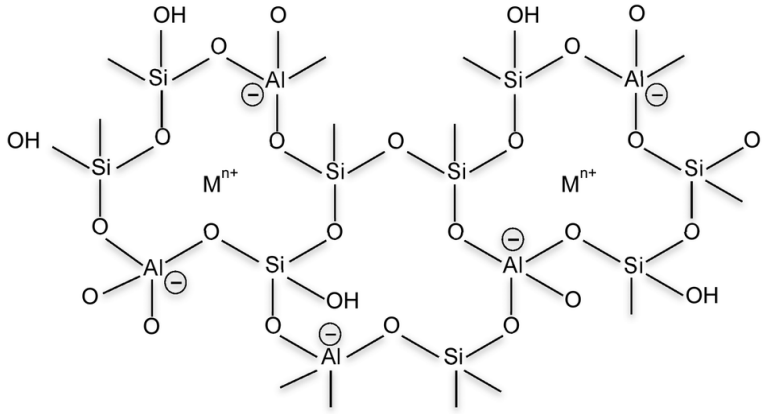

Figure 1: The elementary structural motive of an aluminosilicate zeolite framework, taken from the literature[18].

A key distinguishing feature of zeolites is that their framework, composed of tetrahedral TO_4 units (where $T = Si, Al$) is three-dimensional (as opposed to being composed of two- or one-dimensional sheets/chains of TO_4 units or smaller clusters or completely isolated TO_4 units), making them a part of the tectosilicate family of ordered silicate materials. Tectosilicates (also called framework silicates) represent the most common mineral type with up to two-thirds of the Earth's crust being composed of minerals from this family (primarily Feldspars, Quartz, and related minerals)[19]. Zeolites represent a subgroup of the tectosilicate family characterized by the presence of channels/pores and cavities in their crystalline framework, that are usually in the range of about 3 – 10 Å (i.e. in the micropore range), which are sufficient dimensions to allow the passage or at least encapsulation of smaller guest species. Zeolite pores are usually characterized by the number of framework-T-atoms their entrances are composed of. As such, we can commonly find zeolites with channels consisting of six-, eight-, ten- or twelve-

membered rings (commonly denoted with 6MR, 8MR, 10MR, and 12MR, respectively). For illustration, see Fig. 2 (taken from the literature[20])

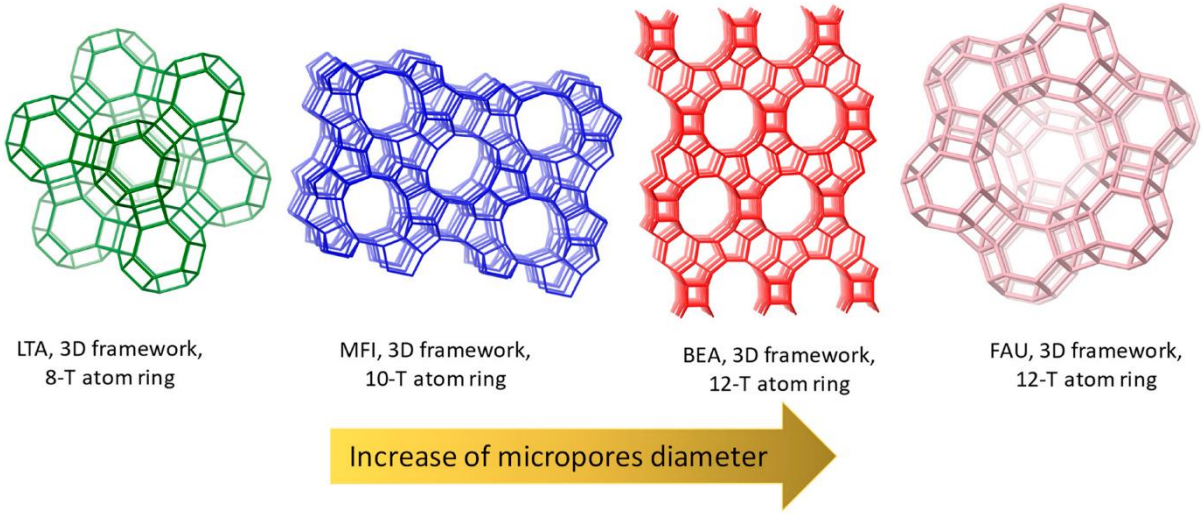

Figure 2: Examples of zeolitic frameworks with various channel sizes, taken from the literature[20].

Despite the fact that researchers working in the field of computational chemistry have been predicting the existence of a very large number of zeolitic frameworks of various chemical compositions[21-23], only 260 distinct fully ordered zeolitic frameworks were reported to have been synthesized according to IZA (along with several dozen partially disordered or intergrown frameworks) as of writing of this text (May 2025)[24]. Each of these frameworks is defined by a set of geometrical motifs formed by the interlinking of their TO_4-units that can be broken down to a small set of fundamental building units. This can be done in several different ways, in particular using the so-called secondary building units (SBUs), composite building units (CBUs), and natural building units (NBUs) (also called natural tiling).

The description using the SBUs assumes that a whole zeolite framework can be broken down into a single fundamental building block, such as a ring, cube or a prism, composed of 3 to 16 T-atoms (the list of which can be found on the website of IZA[25]), which, when periodically connected, yields the whole framework. Such framework decomposition has been done for many zeolite frameworks, but was abandoned by IZA in favor of the other two approaches (using CBUs and NBUs) as of 2007 due to the impossibility to describe newly discovered frameworks using the established set of SBUs – forcing a constant addition of new SBUs, as well as the general inability to intuitively describe characteristic features of a framework (such as large cages of characteristic shapes)[26].

A decomposition of a zeolite framework into the so-called CBUs has been introduced due to the fact that researchers have observed that it would be more practical to break down a zeolite framework not into just a single repeating building unit, but into several types of units (such as cages, channels, chains or layers) representing common structural features of a given framework. The CBUs don't necessarily describe the framework completely and are allowed to overlap. They are usually denoted by a three-character lower-case italic code (e.g. *cha*, *cas*, *pen*, *d6r*), frequently related to the code of the zeolite they describe (see below)[26].

To deal with the fact that the CBUs don't necessarily describe a framework completely, Blatov et al.[27, 28] came up with the idea that a zeolite structure doesn't have to be described by units formed of knots (representing framework T-atoms) and connections (O-bridges) between them, but alternatively by geometrical shapes representing subsets of the 3D Euclidean space. These units (NBUs), all connected in a face-to-face manner, have the advantage of being able to unambiguously divide the 3D space and can therefore be used to unambiguously construct a zeolite framework. Their designation is similar to that of CBUs, except for the addition of an italic *t* before the three-characters (e.g. *t-cha*, *t-cas*, *t-pen*, *t-hpr*). As of now, the description by NBUs is considered to be the best practice[26].

From the paragraphs above, it is clear that developing a systematic nomenclature for zeolitic frameworks is essentially impossible due to their complexity. For this reason, each zeolite framework has been assigned a three-letter capital-case bold code by the IZA (such as **CHA**, **FAU**, **LTA**, **ITR,** or ***BEA** – in the case of the partially disordered frameworks, an asterisk precedes the code). The codes are usually assigned based on previously established trivial names – usually the names of the minerals, in case of naturally occurring zeolites, or the names of various commercial brands or shortcuts of academic institutions where the materials were first synthesized, in the case of the artificially synthesized materials. Many of the trivial names remain in common use, especially in the for-profit sector, but also in academic circles. For example, the **CHA** framework is named after the naturally occurring mineral chabazite, zeolites X and Y are trade names for two materials possessing the **FAU** framework, zeolites 3A, 4A, 5A are trade names for variants of a material with the **LTA** framework and ITQ-1 is a trivial name for **MWW**, named after the Institute of Chemical Technology at the University of Valencia (**I**nstituto de **T**ecnología **Q**uímica).

While there exist over 260 different zeolitic frameworks (when including the partially disordered and intergrown structures), it should be pointed out that only about 38 % of them

occur or have been synthesized in the form of an aluminosilicate, 24 % of them as pure-silica zeolites, 19 % as AlPO or SAPO and as many as 32 % have additionally been synthesized exclusively in a different chemical composition altogether (primarily as germanosilicates or various metal-aluminophosphates - MAPOs)[24]. Of all the frameworks, only a very minor fraction is frequently used for large-scale commercial purposes as of now (primarily **CHA**, **FAU**, **GIS**, **LTA**, **MFI**, **MOR**, **MWW** as well as the partially disordered framework ***BEA**) and as was mentioned at the beginning of this chapter, they are predominantly used as aluminosilicates.

The chemical composition of a zeolite framework can be altered by various post-synthesis modification procedures. These, however, invariably lead to the creation of vacancies/defects within the framework, usually present in the form of hydroxyl (OH) or, less commonly, fluoride (F) groups interrupting the $-O-T-O-$ chains the zeolite framework is composed of – another key feature mentioned in the IMA definition. The existence of these imperfections in the framework isn't necessarily to the detriment of the material's usefulness, as numerous applications based on the use of the zeolite defects exist. The nature of these defect sites (e.g., their acidity) can vary considerably due to steric considerations as well as due to the chemical nature of the atoms surrounding them. For defect hydroxyl groups in particular, it is possible to observe species characterized by various degrees of interaction with their surroundings, such as completely isolated terminal OH groups, OH groups connected to the same T-atom (geminal OH groups), or OH groups located on two adjacent T-atoms (vicinal OH groups). These hydroxyl groups can further be partially or fully H-bonded to one another. A common motif is the so-called "hydroxyl nest", a set of four mutually H-bonded OH groups surrounding a T-vacancy, providing a much more acidic active site than the abovementioned species of hydroxyls. In the case of aluminosilicate zeolites, these "hydroxyl nests" are brought about by arguably the most commonly employed post-synthesis modification in general – the dealumination. This procedure is usually performed by a simple exposure of the zeolite to an acid solution at an ambient or slightly elevated temperature or by steaming in water vapor at elevated temperature[29].

While procedures resulting in the "healing" of defects have also been employed (including by filling the T-vacancies with completely different atoms altogether), their effect is usually limited and a portion of the defects remains, making it necessary to obtain the material of the desired chemical composition directly during the initial synthesis, provided a less defective framework is required.

It has generally been assumed that zeolitic frameworks, unlike MOFs and some other types of microporous materials, represent very rigid structures. This view, however, has been shown not to be entirely adequate in recent years/decades in connection with the observation of intriguing adsorption and thermal behavior in several zeolite systems[30, 31]. The most extreme example of the flexibility of zeolite frameworks is probably observed during the ethene adsorption on ITQ-55 (already mentioned in Section 2)[11], whereby the presence of an ethene molecule has been shown to massively increase the diameter of the pore entrance of the characteristic heart-shaped cage of the material (by up to 30 % according to AIMD calculations), leading to substantial changes in the adsorption kinetics. Another noteworthy example is the flexibility of the **RHO** framework due to both temperature change as well as the presence of guest species (for example, water)[32, 33]. Some forms of **RHO** have been observed to contract their unit-cell volume by over 10 % as a result of relatively mild temperature increases ($\Delta T < 100\ K$)[32], well above the level of deformation observed in most zeolites exposed to comparable changes of state (in which cases the volume changes usually don't surpass 1 %[31]). It should be pointed out that a key feature that brings about the observed volume changes in the case of the **RHO** framework are very often the extra-framework cations located in its channel system.

As was already mentioned, the extra-framework cations (EF-cations) are found in zeolitic materials whose framework bears the negative charge, usually due to the presence of trivalent T-atoms within the framework – most commonly aluminum, but also boron, gallium and others. Despite not being elements of the zeolitic framework per se, very often it's precisely the EF-cations that provide a zeolite with its demanded properties. While the EF-cations aren't connected to the framework by a covalent bond (except in the case of the hydrogen cations), they usually prefer specific locations within the channel/cavity system to minimize the energy of the system. Their localization is closely related to their size (steric limitations) and charge, as well as to the distribution of the trivalent T-atoms within the framework. As such, it is very common that the same zeolitic framework accommodates differently sized/charged cations in very different parts of the channel system, and conversely, the same type of cation can be located in different positions within channels of materials with the same framework but different chemical composition/T-atom distribution.

While the EF-cations largely prefer specific locations, the change of conditions (temperature, pressure, the presence of a guest molecule in the zeolite channel) can significantly alter the equilibrium and divert the cations into different positions, which can lead to drastic changes in observed behavior in, for example, adsorption systems – among the most notable examples of

this phenomenon is the behavior of low-silica **CHA** zeolites interacting with small molecules such as CO_2, CH_4 and N_2, already mentioned[12, 13] in Section 2.

The IMA definition mentions another key feature resulting from the mobility of the zeolite EF-cations, namely their exchangeability by different cations. The ion-exchange (IE) can usually be brought about by a simple exposure of the material to a solution of salt containing the desired cations (in a large excess compared to the quantity of the EF-cations present in the zeolite) at ambient or sometimes slightly elevated temperature, and is often completely reversible, unlike in the case of post-synthetic modifications resulting in the changes within the framework such as dealumination (see above). While the IE is usually reversible, it is not always possible to perform it completely, primarily due to steric considerations – e.g., a small cage surrounded by several trivalent framework atoms might be unable to accommodate a required number of bulkier monovalent EF-cations as opposed to more compact divalent EF-cations.

As was already mentioned on the example of the **RHO** framework, the presence of EF-cations can also have a non-negligible influence on the dimensions of the unit-cell of the crystal framework, provided the framework geometry allows for sufficiently pronounced deformation. This is due to the fact that the positively charged EF-cations are repulsed from each other by electrostatic forces and thus try to maximize their mutual distance within the unit cell, contributing to a slight lengthening of the framework $T - O$ bonds and a change of $T - O - T$ angles.

From the perspective of chemical properties, EF-cations are of acidic character (while the framework oxygen atoms are of basic character) – in the case of metal cations, they represent Lewis acid sites (LAS) (= acceptors of electrons), while in the case of the hydrogen cation, they represent Brønsted acid sites (BAS) (= donors of protons). This chemical character of the EF-cations allows them to interact (or sometimes even react) with various guest species (the interaction energy grows as the basicity of the guest species increases). Additionally, the ability of the EF-cations (as well as of the hydroxyl defects) to strongly interact with guest species elucidates the phenomenon that prompted Cronstedt to give zeolites their name – “boiling stones”. The EF-cations are namely able to bind large quantities of water under ambient conditions, creating relatively stable hydro-complexes. While a large portion of the water molecules present in zeolite pores at ambient conditions usually desorbs already at temperatures below 383 K – accompanied by an observable generation of water vapor noticed by Cronstedt,

provided the zeolite was sufficiently hydrated – removing the most strongly coordinated water molecules can sometimes require temperatures as high as 623 K[34].

Since the introduction of zeolites to the market their consumption has been steadily growing. In 2008, the global zeolite consumption was estimated to be about five million tons, of which slightly over 60 % were natural (mined) zeolites, while the remaining nearly 40 % were of synthetic origin[35]. The whole zeolite market was estimated to stand at about USD 28 billion in 2015[36].

Natural zeolites are primarily used as cement enhancers, nutrient release agents in soil conditioners (exploiting the ability to perform the ion exchange), odor control agents in animal litter (exploiting adsorption properties), as well as drying agents, fillers in paper and plastics and even decontamination agents for radioactive wastewater (by exploiting the zeolite's affinity for ^{90}Sr and ^{137}Cs cations during the ion exchange). The most commonly employed natural zeolite material – used in most of the applications listed above – is clinoptilolite (**HEU** framework)[37].

The synthetic zeolites are used in finer applications requiring materials of higher purity and much more narrowly defined framework structure and/or chemical composition (both with respect to the framework and the EF-cations). The vast majority of the synthetic zeolite consumption is linked to three main types of application – ion exchange, heterogeneous catalysis, and adsorption. Of these three areas, the ion exchange is clearly the largest in scale, wherein zeolites are used as additives in laundry detergent powders, serving as water softeners (based on the ability of the zeolites to replace the Ca^{2+} and Mg^{2+} cations present in water by Na^{+} using the ion exchange). For maximum performance, it is necessary that zeolite ion-exchangers have Si/Al ratios nearing one. As of now, virtually the entire synthetic zeolite ion-exchanger market is based either on the zeolite A (framework **LTA**), zeolite P (framework **GIS**), or, to a lesser extent, on the zeolite X (framework **FAU**). In total, the ion exchange was reported to account for about 72 % of synthetic zeolite consumption in 2008 and a slightly lower fraction of about 65 % in 2015.[36, 37]

While the IE is quantitatively the largest synthetic zeolite application area, heterogenous catalysis makes up the largest portion of the zeolite market value (over 50 %)[37], corresponding to about 17 % of the total synthetic zeolite consumption in 2008, further slightly increasing to about 18 % in 2015.[36, 37] The synthetic zeolite catalyst market has traditionally been dominated by a single application – the Fluid Catalytic Cracking (FCC) – which represented more than

95 % (*sic*) of the global zeolite catalyst consumption[37] in 2008. This process employs the USY zeolite catalyst, (on the basis of the **FAU** framework) exchanged into the H^+ form and thus containing BAS, essentially representing a solid acid. Despite the huge market prevalence of the FCC, a very large number of other commercial zeolite catalyst applications exist, such as various isomerization, oligomerization, alkylation, aromatization, and other types of reactions. For a more specific illustration, one can mention the selective alkylation of toluene to p-xylene using the zeolite ZSM-5 (**MFI** framework), along with the MTO ("Methanol to Olefins") process, where SAPO-34 (a silico-aluminophosphate with the **CHA** framework) is used as the catalyst[37].

The last major area of zeolite application is adsorption (primarily gas separation, gas purification, and drying). Adsorption represents possibly the most dynamically growing branch of synthetic zeolite applications in recent years – in 2008, about 10 % of the synthetic zeolites were used for adsorption purposes, while in 2015, this figure increased by almost a half to about 14 %.[36, 37] A general survey of adsorption mechanisms and some of the most important commercially implemented zeolite applications have already been given in Section 2.

While in the last decades an enormous body of scientific literature on zeolites as adsorbents has been produced, two areas of potential application are particularly intensely investigated by the researchers, namely, the adsorption of CO_2 (for the purposes of flue gas, natural gas, syngas, and biogas separation/purification, as well as general carbon capture) and the separation of hydrocarbons, especially of olefin/paraffin mixtures. The intense interest in these areas can be evidenced by the large number of recent review papers focusing on both the area of CO_2 adsorption[38-45], as well as on the area of the hydrocarbon adsorption[41, 45-47]. Whereas in the past, the focus of researchers was generally oriented towards the commonly (often commercially) available and easily synthesizable low-silica materials with **FAU**, **LTA** or ***BEA** frameworks or higher silica **MFI** materials, recent advances in zeolite synthesis provide the researchers with a very wide array of zeolitic materials, with respect to their morphology, chemical composition as well as their framework topology[11, 48-51]. The adsorptive properties of most of these recently synthesized zeolite materials remain largely unexplored.

While the previously mainly investigated EF-cation rich low-silica materials have been observed to perform very well in the CO_2 adsorption applications, the high polarity brought about by the large cation concentration in their pores usually leads to highly selective adsorption of moisture, as well as increased costs of regeneration. For this reason, researchers are currently

focusing on the investigation of zeolites with lower polarity which would facilitate the adsorbent regeneration and reduce the competitive water adsorption, while nonetheless retaining a high-selectivity and adsorption capacity towards CO_2.[45] Considerably larger problems are observed when the traditionally studied low-silica zeolites are employed for various hydrocarbon separations, primarily due to the nonpolar character of the hydrocarbon molecules which are thus bound more weakly to the ionic sites than both H_2O as well as CO_2. This relatively unsatisfying performance can, however, be drastically elevated by the use of small-pore materials boasting electro-neutral frameworks (such as pure-silica and aluminophosphate frameworks) composed of appropriately sized channels to effectuate a primarily kinetics-driven hydrocarbon separation[11, 52-57]. Such materials not only exhibit an exceptionally high selectivity for appropriate applications, but are also of hydrophobic characters and tend to interact very weakly with the undesirable CO_2 impurity.

4. AIMS OF THE THESIS

This doctoral thesis is generally occupied with the two research problems mentioned at the end of the last section, namely the selective adsorption of CO_2 and the separation of light hydrocarbon mixtures. Within the scope of this thesis, a number of phenomena important for these two fundamental research problems were investigated. The main research aims can be summarized as follows:

1) **The investigation of the influence of different types of hetero-atoms present in the framework of CHA zeolites on the CO_2 and CH_4 adsorption.** Since the vast majority of employed zeolites are aluminosilicates, materials characterized by frameworks composed of different *T*-atoms haven't generally been previously investigated with respect to the CO_2/CH_4 adsorption. Considering that the **CHA** framework can be synthesized with various types of *T*-atoms in its framework[58], it was selected as an appropriate system for the study of the direct influence of the framework chemical composition on the CO_2/CH_4 adsorption. In this work, the pure-silica Si-**CHA**, as well as hetero-substituted B-**CHA**, Al-**CHA** and Ga-**CHA** materials, all in the H^+ form, were investigated.

2) **The investigation of the localization (based on their type and quantity) of alkali-metal EF-cations present in the CHA framework and their influence on the CO_2 and CH_4 adsorption in the CHA (and LTA) systems.** While the very cation-rich low-silica zeolites (Si/Al → 1) usually contain the EF-cations in regularly repeating positions, making them thus detectable via PXRD or other crystallographic methods, the less polar medium- or high-silica materials generally don't contain their EF-cations in such highly regular arrangements, making it necessary to employ other approaches to describe their localization in the zeolite pore – a key parameter influencing the nature of the adsorption of gas molecules on the EF-cationic active sites. In this work, the localization of the EF-cations (Li^+, Na^+, K^+) present in the high-silica **CHA** zeolites (Si/Al > 8.0), as well as in the low-silica **CHA** (Si/Al = 2.1), was investigated. The alkali-exchanged high-silica **CHA**, in addition to the medium-silica **LTA** zeolites (Si/Al = 4.5), were furthermore subjected to a very comprehensive investigation of their CO_2 and CH_4 adsorption behavior, which was clearly shown to be strongly influenced both by the quantity, as well as by the type of the EF-cation.

3) **The investigation of the influence of the framework topology (pore size and shape) of electroneutral zeolite frameworks (CHA and materials synthesized by the ADOR process) on the CO_2 and light hydrocarbon adsorption.** Whereas the EF-cations usually have the decisive role in the processes seeking to selectively adsorb CO_2, electroneutral frameworks characterized by their narrow channels can likewise exhibit very selective behavior towards CO_2, brought about by the maximization of the non-specific interactions. An even more pronounced influence of the framework topology on the adsorption can often be observed in the case of various light hydrocarbon molecules, where very minor structural differences in hydrocarbon isomers can lead to massively different mass-transport behavior in the channel system of a zeolite material possessing an electroneutral framework. In this thesis, a set of novel materials synthesized by the so-called ADOR process[49] (see the next section), characterized by different pore-sizes while retaining a very similar general structure of the layers, was employed to study the influence of the framework topology on the CO_2 adsorption. This set of materials (along with the Si-**CHA**) was furthermore tested with respect to the propane/propene adsorption (in the case of Si-**CHA**, all C_1–C_4 hydrocarbons).

4) **The investigation of the anomalously high selectivity towards propene in the propene/propane separation on the PCR zeolite synthesized by the ADOR process.** One of the materials studied within Aim 3) of this thesis, namely the **PCR** material (characterized by a pair of connected perpendicular 10MR and 8MR channels forming a 2D pore system), was found to exhibit an extraordinarily different adsorption behavior with respect to propene (where a sizeable amount is adsorbed at reasonable rates) and propane (where the adsorption is extremely slow). Furthermore, according to the molecular simulations, no mass-transport blocking was predicted to take place for neither of the two molecules. In this work, a thorough investigation, employing various advanced experimental approaches, was performed on a number of different **PCR** batches in order to elucidate the experimentally observed unexpected behavior of the material.

5. INVESTIGATED SYSTEMS

A summary of the key physical properties of the gas molecules used in this doctoral thesis is in the Table 1 (the values of T_B, T_c, M and d are mostly taken from Poling et al.[59], while the values of the dipole moment, quadrupole moment, and polarizability are taken from the NIST.gov databases[60-62], other references are specified in the table).

Table 1: The basic physical properties of the gas molecules studied in this doctoral thesis.

Gas	T_B (K)	T_c (K)	M (g/mol)	d (Å)	Dipole moment (D)	Quad. moment (D Å)			Polarizability (Å^3)
						Q_{xx}	Q_{yy}	Q_{zz}	
CO	81.7	132.9	28.01	3.690	0.112	1.42	1.42	-2.84	1.953
CO_2	-	304.1	44.01	3.941	0.000	2.14	2.14	-4.28	2.507
CH_4	111.7	190.6	16.04	3.758	0.000	0.00	0.00	0.00	2.448
C_2H_6	184.6	305.3	30.07	4.443	0.000	0.34	0.34	-0.67	4.226
C_2H_4	169.4	282.3	28.05	4.163	0.000	-3.16	1.48	1.67	4.188
C_3H_8	231.0	369.8	44.10	5.118	0.084	-	-	-	5.921
C_3H_6	225.5	364.9	42.08	4.678	0.363	0.60	2.90	-3.50	5.990
n-C_4H_{10}	272.7	425.1	58.12	4.687	0.090	-	-	-	8.020
i-C_4H_{10}	261.3	407.9	58.12	5.278	0.132	-	-	-	8.009
1-C_4H_8	266.9	419.5	56.11	4.46[47]	0.359	-	-	-	7.830
E-2-C_4H_8	274.0	428.6	56.11	4.31[47]	0.000	-	-	-	7.880
Z-2-C_4H_8	276.9	435.5	56.11	4.94[47]	0.257	-	-	-	-
i-C_4H_8	266.2	417.9	56.11	4.84[47]	0.503	-	-	-	7.880

Looking for example at the CO_2 and CH_4, it is clear that that the strongest possible separation effect has to be based on the very large difference between quadrupole moment values of the two molecules, ideally further enhanced by exploiting the difference in the shapes of the molecules (the bulkier CH_4 molecule might have more problems accessing some adsorbent pores than the linear molecules of CO_2). CO, on the other hand, might be disproportionately adsorbed compared to CH_4 due to its nonzero dipole moment. Regarding the mixtures of C_2, C_3, and C_4 hydrocarbons, respectively, achieving a sufficient separation performance in adsorption processes is particularly difficult, as the properties of the respective compounds are very similar. This, however, holds even more true in the case of the conventional distillation process (see Section 1) – the boiling points of propane and propene differ by about 5.5 K, while in the case of the C_4 hydrocarbons, all the relevant molecules have boiling points within a temperature interval of only about 15 K (with for example the boiling points of 1-butene and isobutene differing only by 0.7 K, and those of the 2-butene isomers differing by 2.9 K). Nonetheless, the otherwise very similar molecules generally exhibit differences in kinetic diameters as well as in shape, which can consequently be exploited in kinetically-driven

adsorption processes – provided the adsorbent boasts a homogenous system of pores of dimensions such that the transport of differently sized molecules is hindered to different extents.

The adsorption of these gases was investigated on two main types of zeolitic materials in this doctoral thesis – on zeolites with the commonly available **CHA** and **LTA** topologies of various chemical compositions, and on novel pure-silica zeolites synthesized by the so-called ADOR process.

Both the **CHA** (see Fig. 3) and the **LTA** (see Fig. 4) frameworks possess highly symmetric topologies – the unit cells of both frameworks can be generated by symmetry operations from just a single *T*-atom and four or three oxygen atoms, respectively. These unit cells can be decomposed into the characteristic *t-cha* cages and double-six rings (D6R, or *t-hpr* in tiling), in the case of the **CHA** framework, and into the *t-grc* main cages, *t-toc* sodalite cages, and linking double-four rings (D4R, or *t-cub* in tiling), in the case of the **LTA** framework. For both frameworks, the voluminous but empty main cavities (*t-cha* and *t-grc*, respectively) are connected to each other only through relatively narrow 8MR windows – each cavity boasts six such openings. This structure provides these frameworks with an interconnected three-dimensional channel system characterized by a relatively large pore volume, which is constantly interrupted by narrow "bottleneck" choke points. Such topologies are particularly suitable for adsorption applications as the large cages can lead to a maximization of gas uptake, while the 8MR windows can hinder or completely block the transport of sufficiently large guests – such as for example propane and to a lesser extent propene (as demonstrated in literature on the pure-silica Si-**CHA** material[52, 53]).

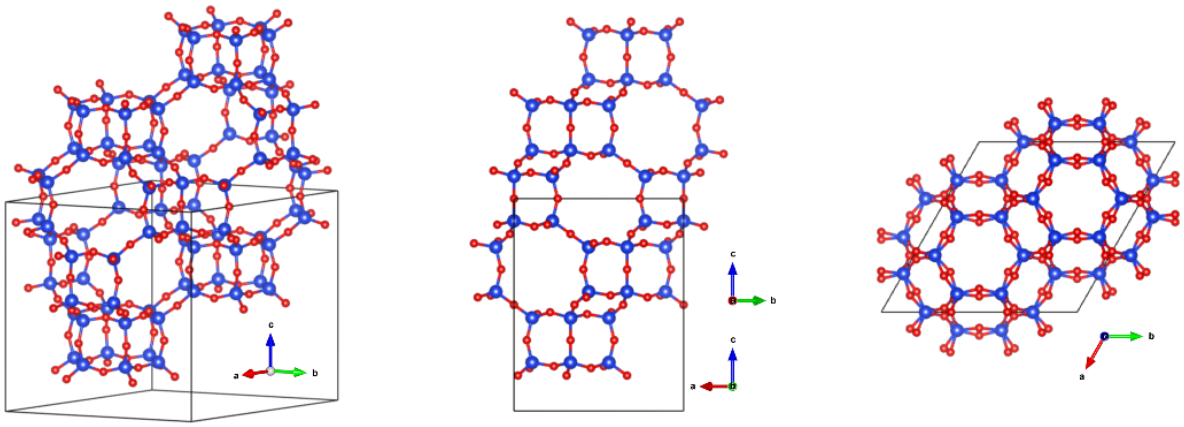

*Figure 3: The framework of the **CHA** zeolite (blue = T-atom, red = oxygen atom).*

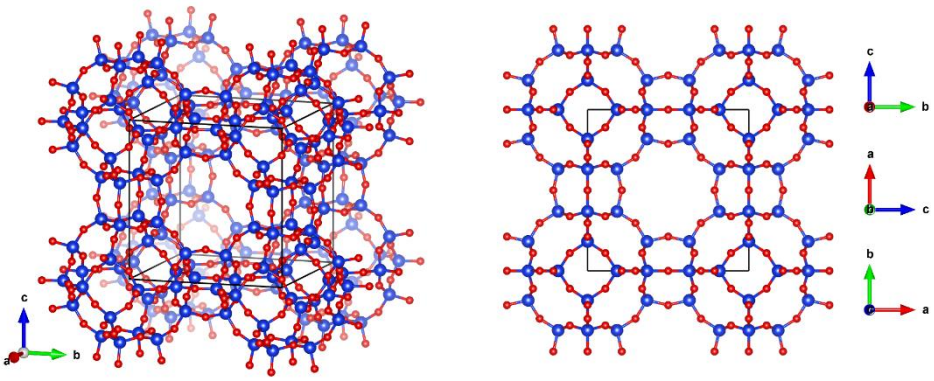

*Figure 4: The framework of the **LTA** zeolite (blue = T-atom, red = oxygen atom).*

Furthermore, the **CHA** framework, in particular, exhibits an exceptional variability when it comes to its chemical composition – in addition to the aluminosilicate and pure-silica forms, the aluminophosphate (AlPO-34), the silico-aluminophosphate (SAPO-34), various other metal-aluminophosphates (MAPO-34)[63], and other rarer isomorphously substituted variants such as borosilicate, gallosilicate and titanosilicate[58] **CHA** materials have been synthesized. The aluminosilicate **CHA** framework was reported to exist (either synthesized or found in nature) in more or less the whole Si/Al range of 1 to ∞, making it possible to acquire adsorbents of the required cation concentration[64]. Concerning the **LTA** framework, its most common low-silica (Si/Al → 1) variants have already been studied to a great detail, and as such, this work will focus exclusively on the as-of-yet generally unexplored properties of the **LTA** materials with medium Si/Al ratios (in the range of 4 to 5).

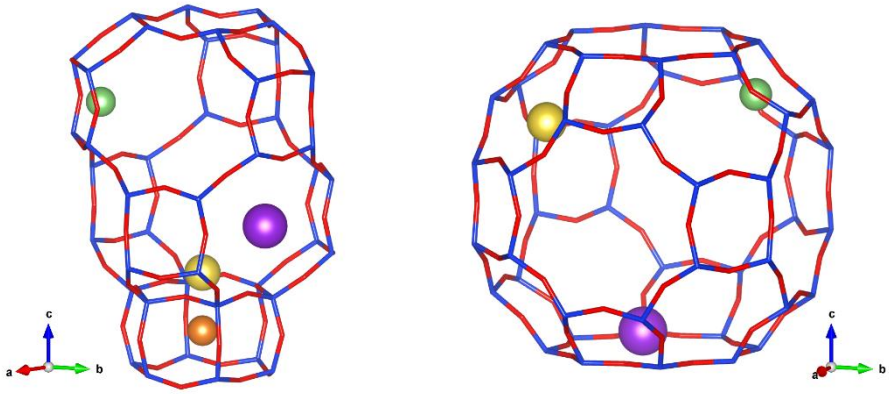

*Figure 5: The EF-cation positions within the **CHA** (left) and **LTA** (right) framework (purple = inside the 8MR, yellow = above the 6MR, green = above the 4MR, orange = inside the D6R).*

Due to their very symmetric topologies, both the **CHA** and the **LTA** frameworks generally possess only several distinct positions in their pore system liable to contain EF-cations (see Fig. 4). These positions include the 8MR window (the site is denoted as SIII' in **CHA** and SII in **LTA**), the space above the 6MR window (SII in **CHA** and SI in **LTA**), the space above the

4MR window (SIII in both **CHA** and **LTA**), in addition to the site inside the D6R of **CHA** (SI). Of these, the positions in the middle of the 8MR window are of particular interest, as their occupancy by sufficiently large EF-cations (such as potassium or cesium) can effectively block the windows for incoming guest-molecules[12]. Nonetheless, even the cations localized in other sites can exhibit a major influence on the adsorption of the guest-species – particularly those possessing a dipole or quadrupole moment (such as CO or CO_2).

The above-listed features – the characteristic framework topology and the EF cation localization (as well as the high variability in chemical composition in the case of **CHA**) – provide the **CHA**- and **LTA**- based materials with an exceptional versatility for a wide range of adsorption (and other) applications, particularly in the fields of CO_2 and light hydrocarbon adsorption. In the scope of this doctoral thesis, materials based on these frameworks were employed in the study of the CO_2 and CH_4 adsorption – with both the influence of the hetero-*T*-atom type (Aim 1), as well as the EF-cation type and quantity (in the case of aluminosilicates) being investigated (Aim 2) – while the **CHA** framework in particular was further investigated for the purposes of light (C_1 – C_4) hydrocarbon adsorption, prompted by the very promising previously published findings[52, 53] (as a part of Aim 3).

The second group of materials employed in this work consists of zeolites that have been synthesized by the so-called ADOR (Assembly-Disassembly-Organization-Reassembly) process[49, 65-67] (for illustration, see Fig. 6, taken from the literature[68]). The ADOR procedure is a recently discovered top-down synthesis method, specifically developed for germanosilicate zeolitic frameworks (e.g. **UTL**[69], **UOV**[70], **IWR**[71], or **IWW**[72]), which possess a characteristic layer-like structure where the hydrolytically unstable germanium atoms are predominantly localized in the D4R (*t-cub*) units serving as pillar-like elements between the "layers".

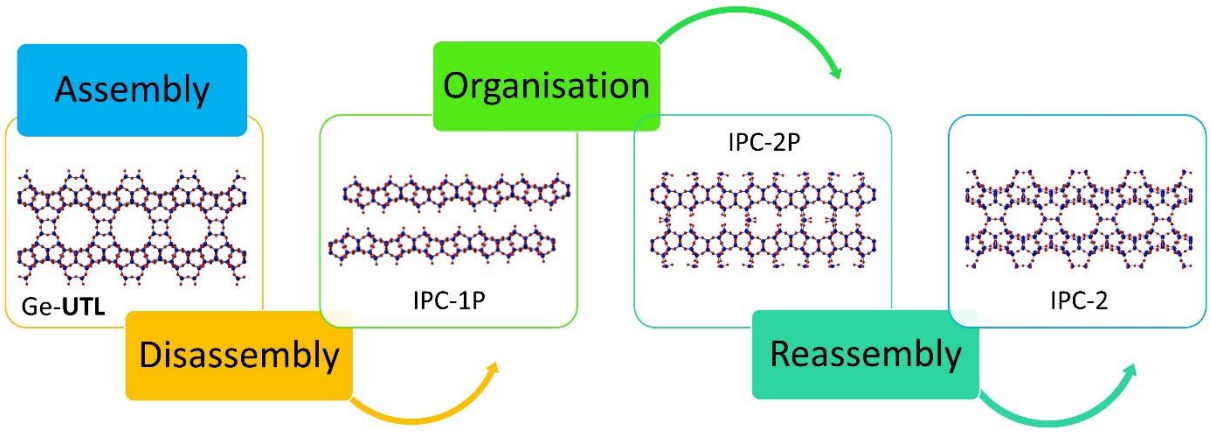

Figure 6: An illustrative example of the ADOR procedure, taken from the literature[68].

In the course of the procedure, the germanosilicate precursor is hydrolyzed into layers, which are then exposed to various changes in physicochemical conditions (pH, presence of specific organic solvents, etc.) before being finally calcined, leading to a reconnection of the as of then "reorganized" layers to form a new pure-silica structure (which usually contains very small amounts of indissoluble residual germanium). The materials synthesized by this approach thus share the same layers as the precursor, but are connected by different, smaller, linking units (such as S4R or merely oxygen bridges), and therefore exhibit smaller interlayer distances than the germanosilicate parent. The ADOR process has already been employed to synthesize a relatively wide array of materials, some of which have never been obtained prior in a direct solvothermal synthesis procedure[65, 73]. Several of these heretofore unobtainable structures were investigated within the scope of this doctoral thesis, which thus contains some of the first ever published results on the adsorption behavior of the materials synthesized exclusively by the ADOR procedure. More specifically, the work presented in the doctoral thesis focuses on materials of the **UTL**[69] and **UOV**[70] germanosilicate precursor families.

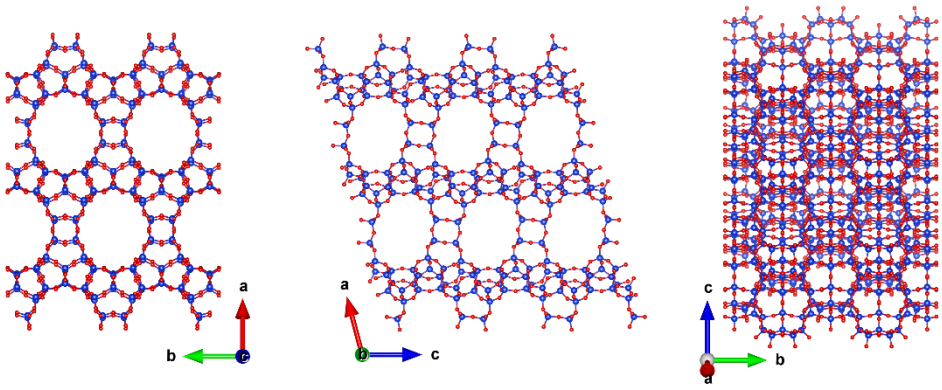

*Figure 7: The framework of the **UTL** zeolite (blue = T-atom, red = oxygen atom).*

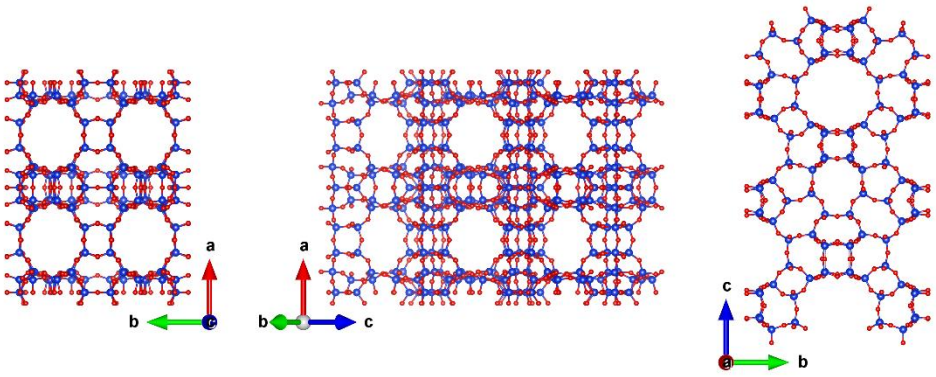

*Figure 8: The framework of the **UOV** zeolite (blue = T-atom, red = oxygen atom).*

The structures of both of the parent frameworks are shown in Fig. 7 and Fig. 8 respectively. For both frameworks, the characteristic layer-like segments extend along the y-z plane and are connected by D4R elements. The orientation of the "layers" and the "pillars" provides both structures with a two-dimensional system of mutually intersecting channels (14 × 12MR in the case of **UTL**, and 12MR intersected by parallel 10 and 8MR channels in the case of **UOV**). In the case of **UTL**, the layers themselves are compact and don't contain additional pores, which is not the case for the **UOV** material, where the layers further contain differently shaped 12MR and 8MR channels (making the channel system of the **UOV** framework three-dimensional). This structural difference subsequently leads to wildly different adsorption behavior not only for these two materials themselves, but also for all of their daughter structures generated by the ADOR procedure.

An overview of all the daughter structures of the **UTL** precursor is in Fig. 9 (taken from the literature[74]). Of all these materials (each denoted by IPC-n, after the **I**nstitute of **P**hysical **C**hemistry of the Czech Academy of Sciences) it was primarily the IPC-4 (synthesized for the first time by the ADOR process[65], since then designated as **PCR** by IZA) that was the object of study within the scope of this doctoral thesis. This was due to its relatively high stability compared to most other ADOR-synthesized materials (in particularly compared to the IPC-9 and IPC-10 featuring uncommon 9MR and 7MR in their frameworks[73]) as well as its small pore size (10 × 8MR channel system, created by the substitution of the D4R pillars in **UTL** by simple oxygen bridges), in the range of kinetic diameters of small gas molecules.

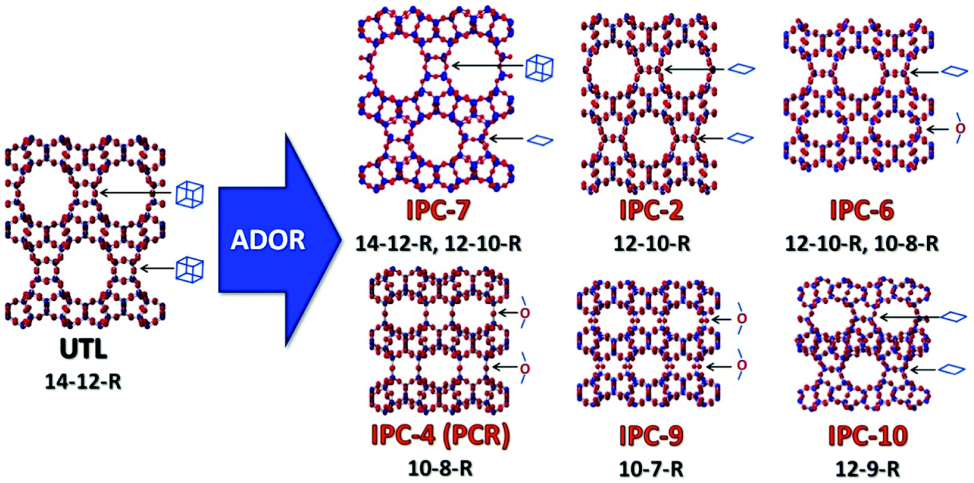

*Figure 9: The **UTL** family of ADOR-synthesized zeolite structures, taken from the literature[74].*

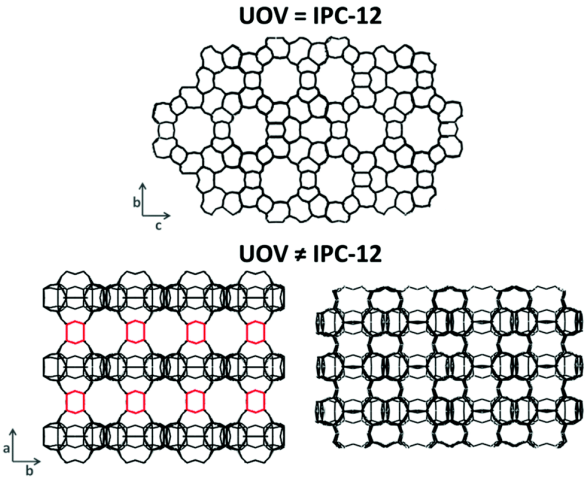

*Figure 10: The IPC-12 zeolite synthesized by the ADOR-procedure from the **UOV** precursor, taken from the literature*[75]

The final material investigated in this thesis was the IPC-12 zeolite[76] synthesized from the **UOV** precursor (see Fig. 10, taken from the literature[75]) by effectively substituting the pillar D4R of the parent by oxygen bridges (making it the **UOV**-family equivalent of the **PCR** zeolite in the **UTL**-family).

The above-listed ADOR structures – **OKO** (IPC-2), **PCR** (IPC-4), IPC-9, IPC-10 and IPC-12 – as well as their precursors, were employed for the study of CO_2 adsorption. This set of materials was deemed particularly suitable for the investigation of the influence of the pore system topology and, in particular, of the channel width (and thus the level of confinedness) on the adsorption of CO_2 (within Aim 3). The **UTL**-family materials were furthermore employed for the purposes of propane and propene adsorption, as the pore-sizes of particularly the **PCR** (IPC-4) and IPC-9 were known to be very similar to those of other pure-silica zeolites known for exhibiting very high propene/propane kinetics-driven adsorption selectivity[52-57] (likewise within Aim 3). This investigation led to a partial confirmation of these expectations based on literature, with particularly the **PCR** exhibiting an extraordinarily selective behavior, which was furthermore not predicted by the computational results. This disagreement between the otherwise very robustly compatible theoretical/computational and experimental approaches required further, much more detailed investigation of the adsorption behavior of this framework vis-à-vis the C_3 hydrocarbons (comprising the Aim 4 of this thesis).

6. EXPERIMENTAL METHODOLOGY

The experimental methodology employed for the purpose of achieving the aims defined within the scope of this thesis consists primarily of direct quantitative measurements of both the adsorption equilibria as well as the adsorption kinetics by means of either volumetric or gravimetric methods. Depending on the specific adsorbent-adsorbate system and the research question, these quantitative measurements were further complemented by additional spectroscopic (typically FTIR spectroscopy), microcalorimetric, or diffractometric (powder X-ray diffraction) experiments (in addition to the other conventionally employed characterization methods such as various techniques for the determination of the chemical composition, SEM imaging, and measurements of nitrogen isotherms at 77.3 K for the textural properties characterization).

The volumetric and gravimetric techniques are primarily used to obtain the adsorption isotherms – pressure dependencies of adsorbed amount – for given adsorbate-adsorbent systems at isothermal conditions (see Eq. 1), but in some cases they can also be used to collect time-resolved uptake curves for separate doses. The setups for both techniques function largely on the same principle (see Fig. 11 for the general schematics of apparatuses used for both techniques).

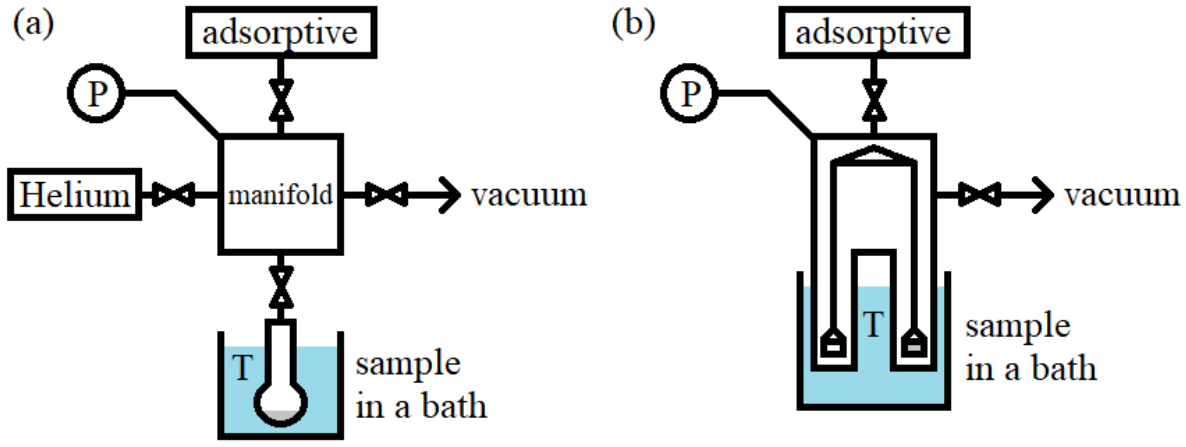

Figure 11: General schematics of the setups used for volumetry/manometry (a) and gravimetry (b)

In each case a vacuum line is used that allows the sample to be exposed to a controlled pressure of the adsorptive. For gravimetry, the adsorbed amount at each dose is determined directly by a microbalance, while in the case of volumetry, it is necessary to calculate the adsorbed amount using the recorded values of pressure.

Each experiment at gravimetry consists of the following steps: (1) A sample is put into a basket that is hung on one side of the microbalance (a metal counterweight is hung on the other side). (2) An in-situ thermal treatment of the sample under high vacuum (< 10^{-3} torr) is performed until the measured weight of the sample remains constant. When the sample activation is finished, the tube containing the basket is put into a thermostat. The system is then left to equilibrate until the desired temperature is reached and the microbalance reports a constant weight. (3) Pre-defined doses of the gas are added into the system, and for each dose, the adsorbed amount is continuously being scanned by the microbalance (allowing for the measurement of the kinetic uptake curves).

In the case of volumetry, the sample is put into a flask-shaped sample tube and activated at a separate treatment unit beforehand. After the treatment is over, the tube is back-filled with nitrogen gas, allowing for a safe reweighing of the sample tube and a transfer of the tube to the volumetric apparatus. The experiment itself then consists of the following steps: (1) The tube with the sample is thoroughly evacuated for several hours. (2) The free volume of the sample tube is determined from the pressure changes during the expansion of a well-defined amount of helium from the manifold into the sample tube (helium is a non-adsorbing gas, therefore the pressure changes during the expansion into the sample tube are given only by the state properties of the gas phase). The sample tube is then further evacuated to remove all helium. (3) Pre-defined doses of the gas are added into the manifold and subsequently expanded into the sample tube. For each dose, the adsorbed amount is calculated using the values of pressure before and after the expansion, along with the previously determined free volume of the sample tube and free volume of the manifold (determined by a calibration), and a sufficiently accurate equation of state describing the behavior of the gas phase.

The measured adsorption isotherms represent the most basic source of information on a given adsorbate-adsorbent system. In addition to merely providing quantitative information on uptake under different conditions, their shape can provide qualitative information on the nature of adsorption in the system. If the same adsorbate-adsorbent system is studied under different temperatures, the resulting adsorption isotherms can be used to estimate the value of adsorption heat (without measuring it directly with a calorimeter). If, on the other hand, adsorption isotherms of various gases are measured on the same sample at the same temperature, it is possible to estimate the selectivity of the adsorbent for the measured gases with, for example, the help of the ideal adsorption solution theory (IAST) (without actually performing any experiments with gas mixtures).

The machines used in this work were two commercially available volumetric gas analyzers ASAP 2020 Physisorption by Micromeritics (USA) and a home-made vacuum line connected to a microbalance MK5 by CI Precision (UK). All the apparatuses allowed to measure adsorption in the temperature interval of 273 to 333 K (regulated by Peltier thermostat). One of the volumetric devices could use an in-built plugin to continuously record the pressure values to obtain the uptake curves.

In addition to the devices above, a calorimetric setup was employed for some experiments presented in this thesis. This device was used for the direct determination of adsorption heats at isothermal conditions. The setup for this technique (in Fig. 12) is essentially the same as the one for volumetry shown above (Fig. 11a) with the exception that the sample tube is not submerged in an isothermal bath, but is instead put inside an isothermally operated calorimeter that is able to detect very small temperature changes occurring due to processes taking place in the sample tube.

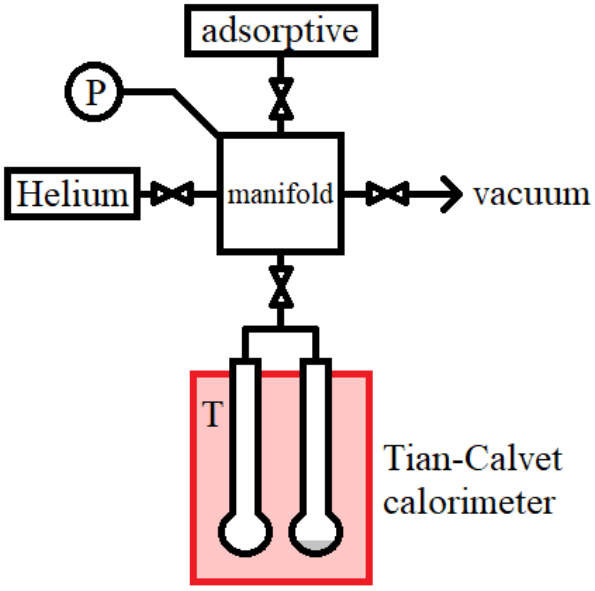

Figure 12: General schematics of the setup used for calorimetry

A BT 2.15 Tian-Calvet-type microcalorimeter by Setaram (France), allowing for experiments at both the room temperature as well as at lower temperatures (with cooling provided by the liquid nitrogen) – all experiments presented in this thesis were performed at isothermal conditions – was used for the determination of the adsorption heats. In order to obtain sufficiently precise results, it is necessary to use an empty reference tube along with the sample tube. The heat released during the adsorption is detected by a 3D fluxmeter sensor consisting of a battery of thermocouples that convert the heat to voltage (using the Seebeck effect). As the

voltage obtained is proportional to the heat-flow, the integrated area under the curve of the obtained time dependency of the signal is proportional to the heat we wish to determine. The constant of proportionality is obtained by calibration and incorporated in the software.

A typical experiment on this setup consists of the same steps as the experiments on purely volumetric setups and yields dependencies of heat flow and pressure on time. These two curves (along with the knowledge of free volume of the tube and manifold and a sufficiently accurate description of the gas phase) can be used to obtain the adsorption isotherm and the calorimetric curve, which shows how adsorption heat changes with growing uptake. This curve can inform us about the nature of adsorbate-adsorbent interactions present in the system, as different types of interactions exhibit widely differing values of adsorption heat.

The remaining home-made setup used for the experiments presented in this thesis is the in-situ Fourier-transform infrared spectroscopy (FTIR) device (see Fig. 13). This apparatus is conceptually very similar to the above described calorimetric setup in that it consists of a home-made vacuum-line connected to an advanced signal detector – in this case an FTIR spectrometer operating in the transmission mode (Nicolet 6700 and Nicolet iS50 FTIR spectrometers equipped with an MCT/D cryo-detector by Thermo Scientific were employed in this work). As such, this setup is able to monitor not only the spectra of the solid samples themselves, but also the spectra of the adsorbed species (at various pressures/saturation, as well as temperatures)

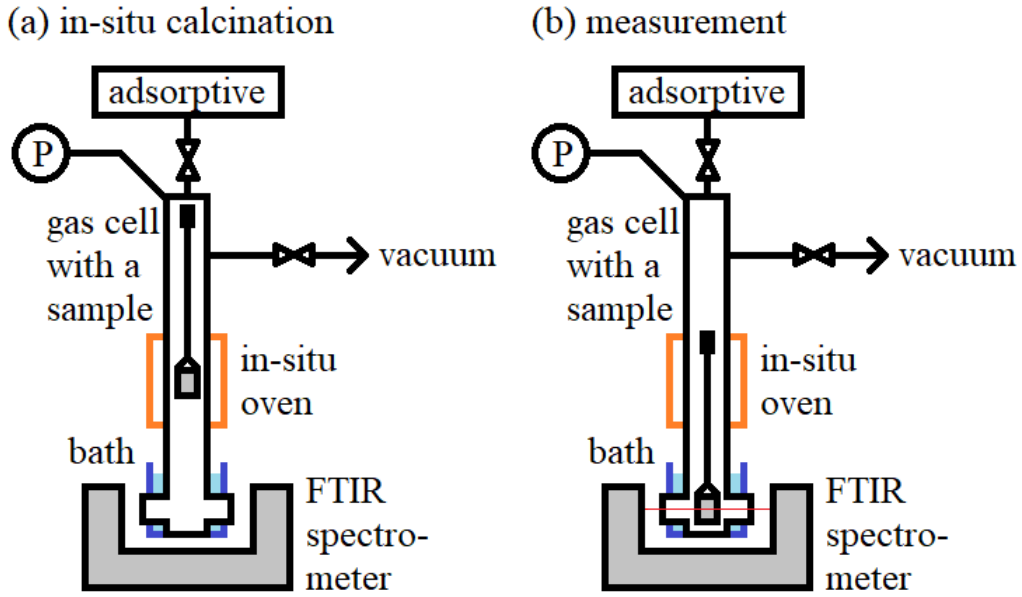

Figure 13: General schematics of the setup used for FTIR spectroscopy, (a) treatment mode, (b) measurement mode

Before each experiment, self-supported wafers of the sample are usually prepared (it is also possible to disperse a small amount of the sample on previously prepared KBr wafers) and

subsequently put into a sample holder. The samples are then subjected to a thermal treatment in an in-situ oven (see Fig. 13a). After the thermal treatment the samples are cooled down to the temperature of the experiment (usually either room temperature or the temperature of the liquid nitrogen) and the measurement itself can begin (see Fig. 13b). First, the spectra of the freshly activated samples are always collected. Then, two general types of experiments can be performed: (1) the measurement of spectra in equilibrium for various pressures of the gas. This type of experiment effectively corresponds to the experiments normally performed at volumetric/gravimetric and calorimetric setups. Alternatively, (2) it is possible to first saturate the activated sample with adsorbate molecules and then record a series of time-resolved spectra during outgassing to obtain information about desorption kinetics of species corresponding to different IR bands.

These experiments allow us to directly study the properties (acidity, localization, quantity, etc.) of the O–H bonds present in the material. Both the hydroxyl groups as well as other types of active sites, such as extra-framework cations, can furthermore be studied indirectly with the help of well-chosen probe molecules, such as carbon monoxide or various nitrile or other probes. The interaction of the probe molecule with distinct active sites usually results in different shifts in vibration frequencies of the probe molecule, allowing us to differentiate between the various types of active sites, to estimate their relative coverages by the probe molecule and, provided we have the time-resolved spectra measured upon desorption, to compare the stability of the complexes formed by the probe and the active site. The experimentally obtained FTIR spectra (as well as the interaction energies as measured by calorimetry) are of key importance when trying to model adsorbate-adsorbent systems by methods of computational chemistry, serving as a bridge between both approaches.

It should be pointed out that all throughout the work on this doctoral thesis, the results were continuously interpreted in a close collaboration with a computational chemistry group of Dr. Ota Bludský from the Institute of Organic Chemistry and Biochemistry (IOCB) of the Czech Academy of Sciences.

7. RESULTS AND DISCUSSION

A relatively large body of interesting results was generated in the course of working on this doctoral thesis. The results will be broadly classified according to the governing mechanism that drives the adsorption preference of some gas molecules over others, investigated in line with each of the four aims of the thesis, as defined in Section 4. While such a classification represents somewhat of a simplification, in this work it was generally speaking possible to class the observed results into three categories depending on which structural feature of the zeolite material was primarily responsible for the observed adsorption preferences: a) the dominant influence of the chemical composition of the zeolite framework – particularly due to the presence of varying amounts of EF-cations and other structural motives brought about by the presence of uncompensated negative charge in the framework (investigated to achieve Aim 1 and Aim 2), b) the dominant influence of the framework topology – in particular the size of the pore entrance windows, as well as the shape and volume of the pores themselves (investigated to achieve Aim 3), and c) the dominant influence of the defects and impurities in the zeolite framework (investigated to achieve Aim 4).

7.1. Preferred adsorption due to framework composition

The chemical composition of the zeolite framework is usually the most important factor influencing the adsorption of small polar molecules (such as CO or CO_2) on the zeolite materials, in particular in the systems where no kinetic restrictions are present. Materials containing different types of atoms in their otherwise identical frameworks can exhibit observable differences in the unit cell dimensions, or in the framework flexibility, which can lead to changes in the adsorption behavior[30]. The most significant influence on adsorption is, however, generally due to the presence of EF-cations, localized in the channel system due to the uncompensated negative charge of the framework generated by the presence of usually trivalent *T*-atoms such as aluminum (as was already explained in Section 3, the quantity of the EF-cations is directly proportional to the quantity of trivalent framework atoms).

The first presented study, performed to achieve Aim 1 of the thesis, investigated the influence of the hetero-atom type present in the **CHA** framework on the adsorption of CO_2 and CH_4. The study was performed on a series of four samples of different framework compositions – a pure-silica material denoted as Si-**CHA**, and three materials containing hetero-atoms, denoted as B-**CHA** (Si/B = unknown), Al-**CHA** (Si/Al = 17), and Ga-**CHA** (Si/Ga = 26) (each possessing charge-compensating H^+ cations).

The adsorption isotherms of CO_2 and CH_4 measured on the samples can be found in Fig. 14. For all materials, a clear preference for CO_2 over CH_4 was observed. This general preference was due to the comparably stronger interaction of CO_2 with the relatively polar framework of the zeolites due to the large quadrupole moment of CO_2 – leading to a large value of $\phi_{\dot{F}Q}$ in the case of the CO_2 adsorption (and zero $\phi_{\dot{F}Q}$ for CH_4 as it possesses no quadrupole moment).

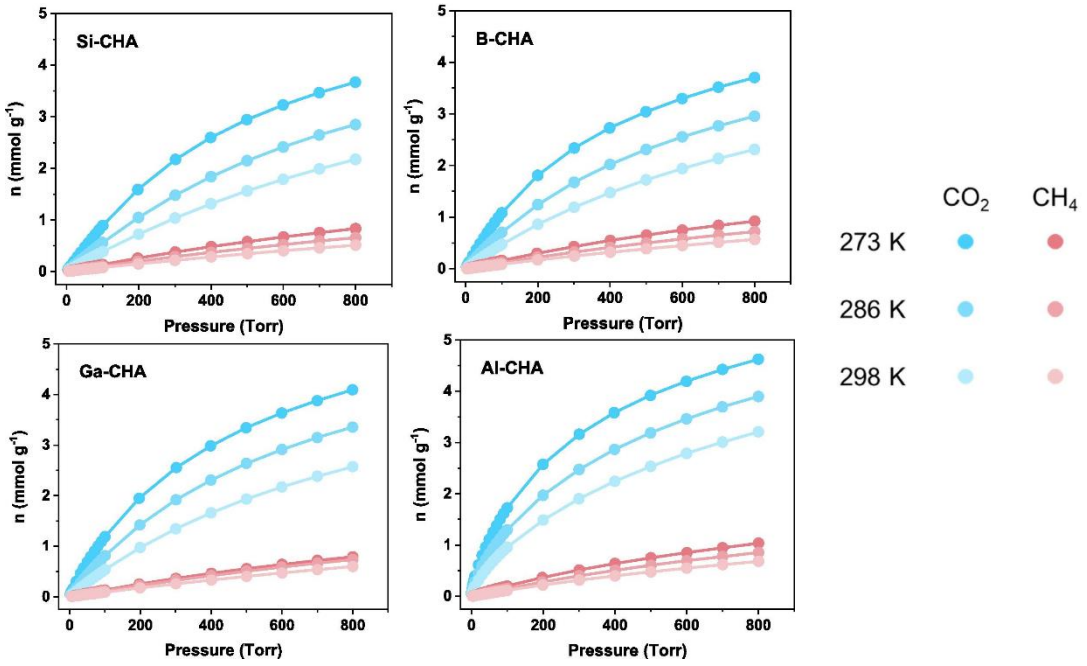

*Figure 14: Single-component adsorption isotherms of CO_2 and CH_4 at 273, 286, and 298 K on M-**CHA** (M = Si, B, Al and Ga).*

This preference was furthermore intensified in the case of the Ga-**CHA** and especially Al-**CHA** (as well as possibly in the case of B-**CHA**) due to the presence of EF H^+ cations (as these materials contained trivalent *T*-atoms), which further increased the electric field gradient at the surface of the material, leading to a stronger interaction with the quadrupole moment of the CO_2. While the CH_4 adsorption was also observed to increase for these materials (except in the case of the Ga-**CHA** isotherm at 273 K, likely due to experimental imprecisions) the increase was considerably smaller as it corresponded only to a slight rise in the value of ϕ_{Ind} due to an increase in the electric field of the adsorbent surface (the same effect also partially contributed to the overall increase in the CO_2 uptakes).

These findings were supported by the analysis of the adsorption heats (see Fig. 15) calculated by the isosteric method from the adsorption data presented in the Fig. 14. The values of adsorption heats of CO_2 for Si-**CHA** were constant with uptake and equal to about 24 – 26 kJ/mol in the whole range (the increase at higher coverages likely being caused by the presence of adsorbate-adsorbate interactions), this was perfectly in line with data published in

literature[77]. In the case of B-**CHA**, Ga-**CHA**, and Al-**CHA**, however, it was found that the zero-coverage CO_2 adsorption heats increased to about 26.5, 28, and 31 kJ/mol respectively, with the Al-**CHA** material in particular exhibiting a decrease in interaction energy with increasing uptake.

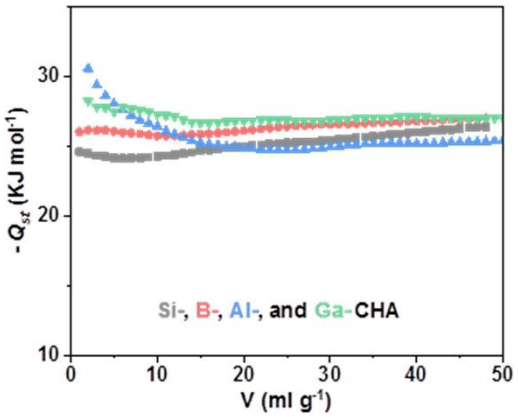

*Figure 15: Heats of adsorption (Q_{st}) of CO_2 on M-**CHA** (M = Si, B, Al, and Ga).*

This behavior corresponded very well with the presence of differently acidic hydrogen cation active sites in the materials. While in the case of the Al-**CHA** material, the observed values (31 kJ/mol) neared those observed on the commercial H-SSZ-13 **CHA** material[78] (about 34 kJ/mol), the lower value observed for the Ga-**CHA** material was expected due the weaker acidic behavior of the $Ga^- - OH^+ - Si$ motive compared to the equivalent motive (Brønsted acid site) in the aluminosilicate materials[79]. In the case of the B-**CHA** material, it was obvious that the heat was higher than in the case of Si-**CHA**, but nonetheless, no clear decrease characteristic for the carbon dioxide interaction with the extra-framework hydrogen cations was observed.

In order to gain further insight into the mechanism of the interaction, the in-situ FTIR spectra of the adsorbed carbon dioxide (see Fig. 16 for the asymmetric stretching vibration region of the carbon dioxide molecule) were additionally measured. The spectra revealed essentially three different types of behavior of the carbon dioxide vibration – Al-**CHA** and Ga-**CHA** samples exhibit bands at 2346 cm^{-1}, previously observed on other materials where the CO_2 interacted with the EF H^+ cations (Brønsted acid sites)[80, 81], while the Si-**CHA** exhibited a much weaker band, shifted to 2341 cm^{-1}, which corresponded well with the band observed on other pure-silica zeolites during the CO_2 adsorption[82]. In the case of the B-**CHA** material, the band seemed to be composed of at least two signals – the 2341 cm^{-1} (corresponding to the interaction with the silicate framework[82]) and another signal at a higher frequency, likely corresponding to an acidic site. It was hypothesized that since the tetra-coordinated boron is known to be unstable

in the tetrahedral configuration in the zeolite framework[83], the material could contain a high concentration of structural motives composed of tri-coordinated boron atoms opposed by silanol groups ($B^+ OH - Si$) (generated by a breakup of the $B^- - OH^+ - Si$ groups). Such sites would represent a weaker Lewis acid sites, which would still lead to an increase in the CO_2 adsorption (and the interaction energy), albeit a less significant one than in the case of the EF H^+ active sites.

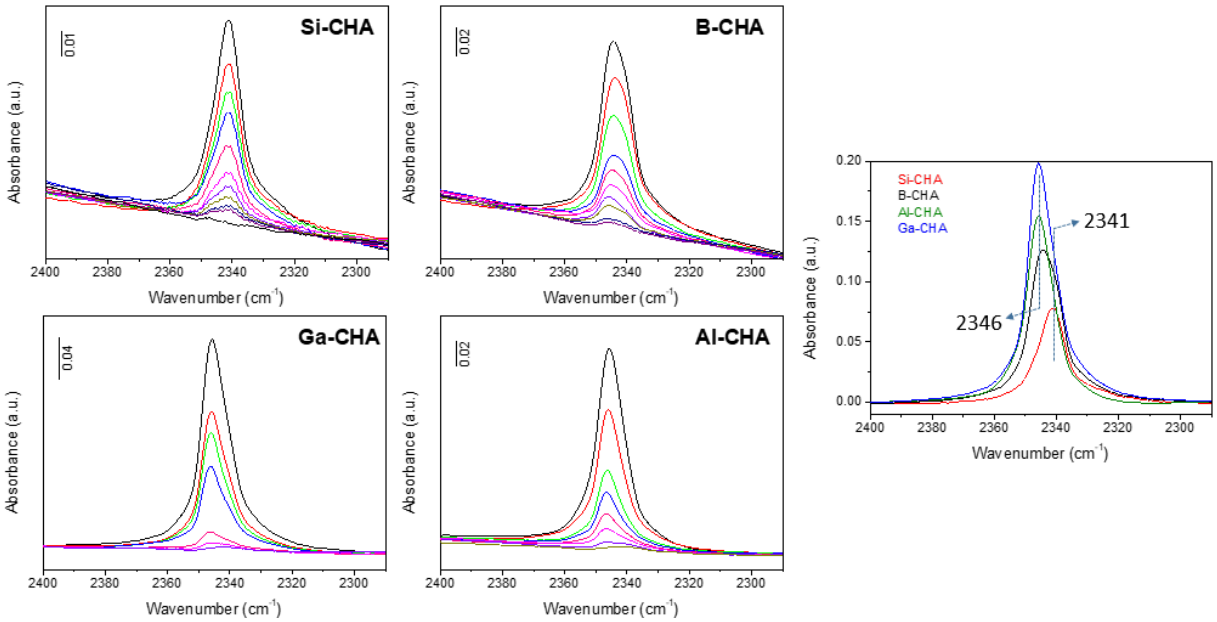

Figure 16: Representative spectra of CO_2 adsorbed on M-CHA (M = Si, B, Al and Ga) as a function of CO_2 pressure (from 0.2 to 8 Torr from bottom to top). Comparison of the adsorbed CO_2 asymmetric stretching vibration (ν_3) at 8 Torr at room temperature on all M-CHA (right)

It has furthermore been observed by analyzing the results from the diffractometric experiments that the introduction of hetero-atoms in the **CHA** framework leads to slight changes in the framework topology – particularly changes in the entrance window dimensions (see Fig. 17). It is possible that the relatively large deformation of the 8MR window in the case of the Ga-**CHA** could additionally contribute to a slight change in the CO_2 uptake, as the CO_2 has been reported to coordinate inside the 8MR window itself[77].

To summarize, this study has demonstrated that the chemical composition of the framework exerts its influence on the adsorption behavior of the zeolite primarily indirectly by means of the EF-cations or other active sites present in the material due to its chemical structure. Of the four presented materials, the Al-**CHA** possesses clearly the most selective behavior while still retaining relatively low values of the carbon dioxide adsorption heat (30 – 35 kJ/mol), potentially allowing for a fairly cheap regeneration of the saturated material. As the

aluminosilicate **CHA** materials are additionally also clearly the simplest and cheapest to synthesize, they seem to offer the highest potential for real-life applications.

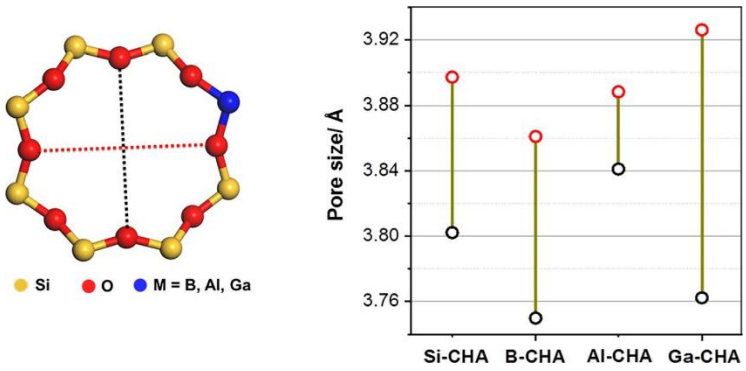

Figure 17: (left) A schematic representation of the 8MR and of the evaluated distances (calculated as crystallographically obtained interatomic distances reduced by the van der Waals radii), (right) the obtained values of the distances.

In order to achieve Aim 2 of this thesis, an extensive investigation of CO_2 and CH_4 adsorption (as well as CO, for the purposes of characterization) on various Al-**CHA**, as well as Al-**LTA** materials has been carried out. The study was performed on samples obtained by the ion-exchanges of four **CHA** zeolite matrices (with Si/Al = 35.4, 16.3, 9.2, and 8.0 respectively) into various alkali-metal forms (Li^+, Na^+, and K^+), as well as on three UZM-9 samples (**LTA** framework with Si/Al = 4.5), likewise exchanged into the three respective alkali-metal cationic forms (Li^+, Na^+, and K^+). From this point on, the materials will be denoted by M-**CHA**-n (or M-**LTA**-n), where M – is the EF cation, and n = Si/Al. The summary of the results obtained on the alkali ion-exchanged **CHA** and **LTA**, along with the results on the materials containing various *T*-atoms, is in the Table 2.

The presence of the EF-cations in the zeolite leads to a rise in the polarizability, electric field and especially an increase in the electric field gradients on the surface of the zeolites. This results in increases in both non-specific dispersion contributions ($\phi_D + \phi_R$), as well as the specific contributions ($\phi_{Ind} + \phi_{F\mu} + \phi_{\dot{F}Q}$) in the gas interactions with the surface. As the CH_4 is a non-polar molecule, the strength of the interaction increases generally only due to effects related to the polarizability of the system (ϕ_D, ϕ_R, and ϕ_{Ind}), leading to a rise by about 3 to 6 kJ/mol depending on the cation in the case of the **CHA** system. For CO_2 on the other hand, the rise in interaction energy (over 15 kJ/mol for all **CHA** samples with alkalic metal EF cations, and by at least 13 kJ/mol in the case of the **LTA** samples, when comparing with literature data on Si-**LTA**[84, 85]) consists not just of the non-specific contributions, but especially due to a massive increase in the $\phi_{\dot{F}Q}$ (owing to the large quadrupole moment of the CO_2). At the very low coverages on some **CHA** materials (with a larger quantity of cations), the

adsorption heat was observed to be up to 30 kJ/mol larger than in the case of the pure-silica material. This was likely due to the appearance of chemisorbed species (carbonates) on some structural motifs within the system (whose ΔH >> 50 kJ/mol).

*Table 2: The summary of CO_2, CH_4 and CO adsorption data on the hetero-substituted and alkali-exchanged **CHA** and **LTA** materials*

Sample	n_{CO_2} [a] (mmol/g)	n_{CH_4} [a] (mmol/g)	S_{CO_2/CH_4} [b] (-)	ΔH_{CO_2} [c] (kJ/mol)	ΔH_{CH_4} [c] (kJ/mol)	ΔH_{CO} [c] (kJ/mol)
Si-**CHA**	2.17	0.51	5.0	24.6 (*)	15.9 (*)	–
B-**CHA**	2.31	0.57	5.7	26.0 (*)	17.2 (*)	–
Al-**CHA** (Si/Al = 17)	3.21	0.68	21.3	30.6 (*)	16.9 (*)	–
Ga-**CHA** (Si/Ga = 26)	2.57	0.60	6.4	28.2 (*)	16.6 (*)	–
Si-**CHA** (batch 2)	2.40	0.55	4.9	23.9	17.5 (*)	16.6
K-**CHA**-35	3.00	0.68	48.1	39.7	–	26.4
K-**CHA**-16	2.95	0.71	71.1	41.2	18.7 (*)	25.9
K-**CHA**-9	3.73	0.86	89.9	–	19.2 (*)	–
K-**CHA**-8	3.59	0.94	100.0	45.4	20.5 (*)	28.8
Na-**CHA**-16	3.10	0.74	50.6	44.1	21.6 (*)	31.7
Na-**CHA**-9	3.95	0.98	95.8	44.3	22.1 (*)	30.8
Na-**CHA**-8	3.93	1.04	140.8	47.5	23.0 (*)	31.6
Li-**CHA**-16	2.95	0.64	140.6	53.2	–	34.8
Li-**CHA**-9	3.88	0.86	222.8	–	–	–
Li-**CHA**-8	3.93	0.90	241.5	56.0	–	35.6
K-**LTA**-4.5	3.63	0.58	188.2	38.0 (*)	17.1 (*)	–
Na-**LTA**-4.5	3.87	0.46	162.7	34.5 (*)	17.6 (*)	–
Li-**LTA**-4.5	4.39	0.44	60.8	34.5 (*)	17.2 (*)	–

[a] – uptake at 800 torr, 298 K measured volumetrically (293 K in the case of **LTA**)
[b] – selectivity at ~zero coverage (5 torr) estimated by IAST for a 1:1 mixture, 298 K (293 K for **LTA**)
[c] – zero coverage adsorption heat measured calorimetrically or by the isosteric method (*)

Interestingly, however, whereas in the case of the **CHA** system, the affinity of the CO_2 for the material grew in the order of $K^+ < Na^+ < Li^+$, corresponding to the strength of the field gradients generated by the respective cations (the smallest Li^+ generates the sharpest gradient, while the largest K^+ creates the weakest one), the observed trend was precisely the opposite in the case of the medium-silica **LTA** system. This shuffling in the CO_2 preferences, which contradicts the simple model assuming the interaction of a single cation with a single CO_2 molecule, has been previously observed on several other types of alkali-exchanged zeolites, such as **FAU**[86, 87] (where the CO_2 interaction energy increases in the order of $Li^+ < Na^+ < K^+$) and **FER**[88] (in which case the adsorption preferences follow the order: $Li^+ < K^+ < Na^+$). This seeming CO_2 preference inversion, observed in the **FAU** system (which closely matches the one observed on the **LTA** frameworks presented herein), was ascribed by the authors of the two studies[86, 87] to

two possible effects: 1) the formation of bridging CO_2 complexes in the K-**FAU** system, 2) the formation of adsorbed CO_2 complexes interacting simultaneously with the EF-cations located in the most exposed cationic sites (preferred by the K^+ cations) and with the adjacent basic oxygens. Considering the structural similarity (size and spherical shape of the cages), as well as the appropriate distance of the 8MR cationic sites in the **LTA** zeolite, it is plausible to assume that such bridging CO_2 species could also be formed in the case of the K-**LTA**-4.5 system (as opposed to the Na-, and especially Li-**LTA**-4.5 systems, whose inter-cationic distances would likely not be appropriate for the formation of these species.

Concerning the quantification of the adsorption performance, it can be said that in the case of **CHA**, the uptakes generally grew with the increasing EF-cation content (within the investigated range of Si/Al ratios). Despite the Li^+ cation exhibiting clearly the strongest interaction with the CO_2 molecules, the Na-exchanged samples generally exhibited a larger uptake of CO_2, which might have been caused by a better accessibility of the cationic sites. The selectivity of the CO_2 over CH_4 (estimated for a 1:1 mixture by the IAST approach) grew with the increasing cation content and in the order of $K^+ < Na^+ < Li^+$, with the most selective sample (Li-**CHA**-8) exhibiting the IAST selectivity of about 240. It should be pointed out, however, that an increase in selectivity was generally accompanied by an increase in the CO_2 adsorption heat, which would consequently increase the cost of adsorbent regeneration in a real process. The **LTA** system generally exhibited comparable uptakes of CO_2 (except for the Li-**LTA**-4.5 material, which exhibited the largest observed CO_2 uptake at 800 torr), its affinity for CH_4 was, however, clearly smaller, which was likely caused the more open structure of the **LTA** pore system resulting in weaker non-specific interactions of the non-polar CH_4 molecule with the framework. Combined with the clearly lower values of CO_2 adsorption heat (resulting in easier regeneration) it is likely that the **LTA** system is more appropriate for real CO_2/CH_4 separation applications than the **CHA** system. An accurate assessment as to which cationic form would perform the best in a real process would have to be performed under real industrial conditions, however, as eventhough the K^+ form is the most selective, its CO_2 adsorption capacity and regenerability is slightly worse than in the case of the Na^+ and Li^+ forms.

In order to gain insight into the EF-cation localization within the **CHA** system, the CO was employed as a probe molecule in calorimetric and in-situ FTIR experiments, which were subsequently discussed and interpreted in light of the molecular simulations performed by the collaborators. The values of CO adsorption heats are in Table 2, while the typical CO vibrational spectra for each cationic form are in Fig. 18.

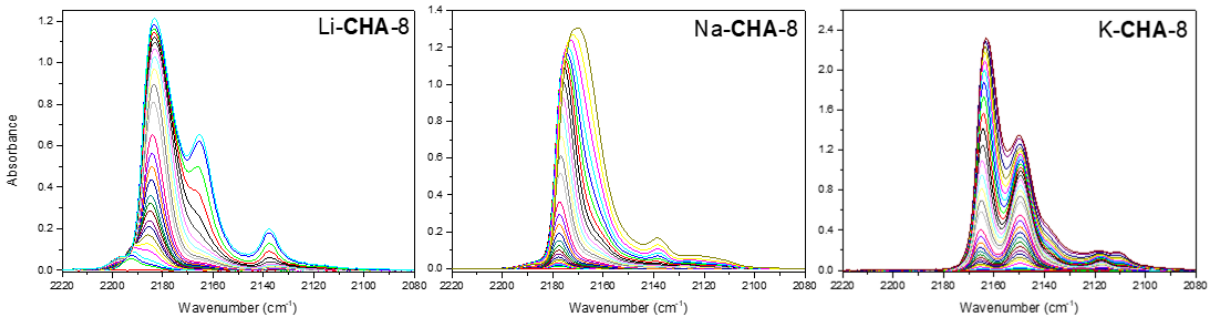

*Figure 18: The vibrational spectra of CO on Li-, Na-, K-**CHA**-8 (time resolved spectra of desorption after equilibration at 0.08 torr, 77 K)*

These investigations revealed that **CHA** materials of Si/Al ratios corresponding up to approximately four aluminum atoms per unit cell (Si/Al ~ 8) were characterized by the presence of clearly localized cationic sites, with the Li^+ and Na^+ cations generally preferring the position above the D6R (SII), while the K^+ cation predominantly favoring the position in the middle of the 8MR (SIII'). This largely confirmed previously published experimental[89, 90] and computational[91] results. These localization preferences weren't absolute, however, particularly as the number of cations in the cell increased. This was clearly visible, for example, in the case of the Li-exchanged zeolites, where at the very low-coverages a band corresponding to CO interacting with Li^+ localized either above the 4MR (SIII site) or inside the 8MR (SIII' site) was found. The CO probe was generally observed to form mono-carbonyl ($M^+ \cdots CO$) or di-carbonyl ($OC \cdots M^+ \cdots CO$) complexes with the alkali-metal cations, although certain configurations also allowed for the creation of bridging carbonyls, where a single CO molecule interacted with two cations at the same time ($M^+ \cdots CO \cdots M^+$). These complexes were clearly observed for the K-exchanged materials (as evidenced by a characteristic band at 2150 cm^{-1}, present in the spectra, as well as an observable increase in the adsorption heat by several kJ/mol), but may have also been present in the Na-exchanged **CHA**.

It should be pointed out that the different site preferences of each cation may have contributed to the observed differences in the CH_4 uptake on the **CHA** materials, as the relatively sheltered SII position above the D6R (heavily preferred by the Li^+) is likely less accessible to a somewhat bulky molecule such as CH_4 than the SIII' position in the middle of the 8MR, which was likely occupied by a comparably larger fraction of the Na^+ cations and the majority of the K^+ cations (leading to a higher CH_4 uptake in the case of these two cations).

To investigate the behavior of the system containing a considerably larger EF-cation quantity in the unit cell, additional zeolite samples were obtained by a direct synthesis and a subsequent

ion-exchange, denoted as K-**CHA**-2 and Na-**CHA**-2 (Si/Al = 2.1, which corresponds to ~12 EF-cations in the unit cell). Their CO vibrational spectra are in Fig. 19.

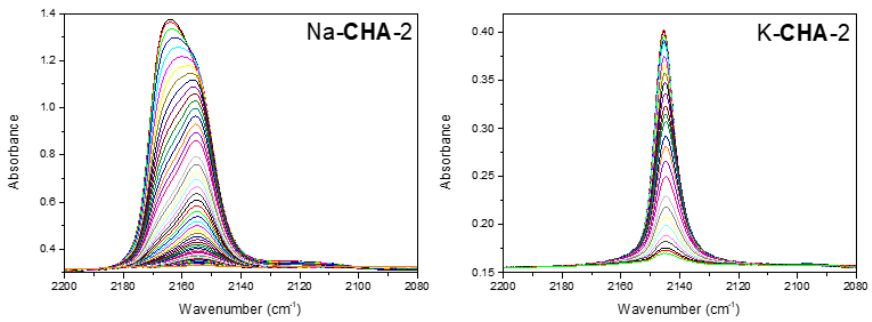

*Figure 19: The vibrational spectra of CO on Na-**CHA**-2 and K-**CHA**-2 (time resolved spectra of desorption after equilibration at 0.08 torr, 77 K)*

Already during the measurement of the spectra, a noticeable difference in the behavior between these two samples was observed. While in the case of the Na-**CHA**-2, the CO adsorption took place very quickly (similarly to all the above demonstrated hetero-substituted and alkali-exchanged materials), for the K-**CHA**-2 material it was necessary to increase the temperature (above the standard 77.3 K used for the experiments) for the saturation to take place. Additionally, the CO vibrational spectra of K-**CHA**-2 exhibit only a single weak band, unlike in the case of Na-**CHA**-2 and all the other previously investigated alkali-exchanged **CHA**.

To describe the behavior observed in low-silica zeolite systems computationally, a statistical approach was required, which involved calculating a large number of structures (due to a large number of possible Al configurations in the framework) and performing molecular dynamics simulations at the DFT level of theory. The results revealed that unlike in the case of the high-silica **CHA**, there is only a very small difference in the SIII' occupancy between the Na^+ and K^+ form of the zeolite (0.80 vs. 0.85), which, however, amounts to a widely different percentage of completely closed off *t-cha* cages (~50 vs ~90 %), explaining the observed obstruction of the pore system in the case of the K-**CHA**-2 material – a gate effect. The results further revealed that while in the case of the Na-**CHA**-2 system, the CO molecule generally remains localized on well-distinguished multiple-Na^+ sites, the K-**CHA**-2 system contains no detectable potential minima for the CO molecules. Further ab initio molecular dynamics (AIMD) computations revealed that a CO molecule localized inside a *t-cha* cage completely closed by K^+ cations isn't localized to any specific position and exhibits a very minor blueshift, precisely matching the experimental observation.

While the ability of the low-silica **CHA** materials (in particular the K-exchanged materials) to kinetically exclude certain molecules by the gate effect (already observed previously in the literature[12, 13]) could lead to an exceptionally high adsorption selectivity in specific applications, their high EF-cation content generally leads to a clear increase in the interaction energy with the adsorbate, commonly due to the generation of chemisorbed species (and thus higher regeneration costs) and a very high affinity towards a wide variety of polar impurities such as H_2O, H_2S and NO_x, when compared with their higher-silica equivalents. In addition, low-silica adsorbents can generally be expected to have considerably reduced adsorption capacities as a large portion of their channel system is already occupied by the EF-cations and is thus unavailable for the gas probes. As such, establishing the optimal chemical composition (Si/Al, and the type of cation) of the **CHA** zeolite to achieve the best performance (an interplay of high uptake, high selectivity, low regeneration costs and cheap synthesis) in a given adsorption or separation application would require investigations under real industrial conditions.

7.2. Preferred adsorption due to framework topology

While the presence of a large quantity of sufficiently large EF-cations positioned inside the channel openings of the **CHA** materials might lead to a kinetic exclusion of some guest species, the framework doesn't necessarily require the presence of these cations for the transport of some gas molecules to be hindered. Indeed, it has been established that electroneutral zeolite frameworks (such as the pure-silica or aluminophosphate variants) of appropriate pore sizes (usually containing 8MR pore entrances) can be exploited for very highly selective kinetically-driven adsorptive separations of, for example, light hydrocarbon molecules[11, 52-57, 92, 93]. Unlike in the case of the systems demonstrated in the last subsection, such differences in adsorption preferences aren't directly caused by the chemical nature of either the framework or the EF-cations present, but predominantly by the geometrical properties of the framework.

Exploiting this mechanism for gas separations is advantageous for several reasons. Firstly, the lack of stronger active sites in the form of the EF-cations means that an interaction with more reactive gas molecules (such as the unsaturated hydrocarbons) is less likely to lead to undesired chemical reactions (such as oligomerization) which would result in a decrease in the yield and the coking of the adsorbent. Furthermore, the relatively weak electric field generated by the silicate framework containing no trivalent *T*-atoms nor EF-cations exhibits much weaker interactions with many commonly appearing impurities such as water, NO_x, H_2S or CO_2 (the adsorption heat of CO_2 measured for Si-**CHA** in the last section was only about 24 kJ/mol), further decreasing the likelihood of the poisoning or the coking of the adsorbent. Finally, while

the lower interaction energy between the gas and the adsorbent leads to a decrease in the adsorption isotherm steepness and thus lower uptakes at the working conditions, the lack of EF-cations in the pore system generally results in a larger fraction of the pore volume being accessible for the gas, partially compensating for the uptake decrease due to the weaker adsorbent-adsorbate interaction.

While these properties seemingly make this mechanism favorable for small hydrocarbon separations, its advantages are largely compensated by the necessity to very tightly control the pore entrance diameter, whose dimensions generally can't be very well tuned (unlike in the case of the chemical composition) as they are connected to the framework topology itself. Moreover, the nature of the mechanism lays further demands on the control of the crystal morphology of the sample – the molecules whose transport into the channel system of the zeolite is hindered will take a longer time to diffuse into larger crystals.

Within the scope of this thesis (more specifically its Aim 3), the light hydrocarbon (C_1 – C_4) adsorption/diffusion was extensively investigated on the already previously mentioned Si-**CHA** material. The uptake curve measurements were performed independently on the two available volumetric and gravimetric setups, allowing the recording of time-resolved uptake data (see Section 6) to verify the reproducibility of the results. The experimental observations were subsequently compared with the computational results obtained by a quantum mechanics-molecular mechanics/transition state theory (QM-MM/TST) methodology developed for the theoretical description of slow diffusion in microporous materials by the collaborators at IOCB. The normalized hydrocarbon uptake curves on the Si-**CHA** sample, measured by both experimental approaches, are in Fig. 20.

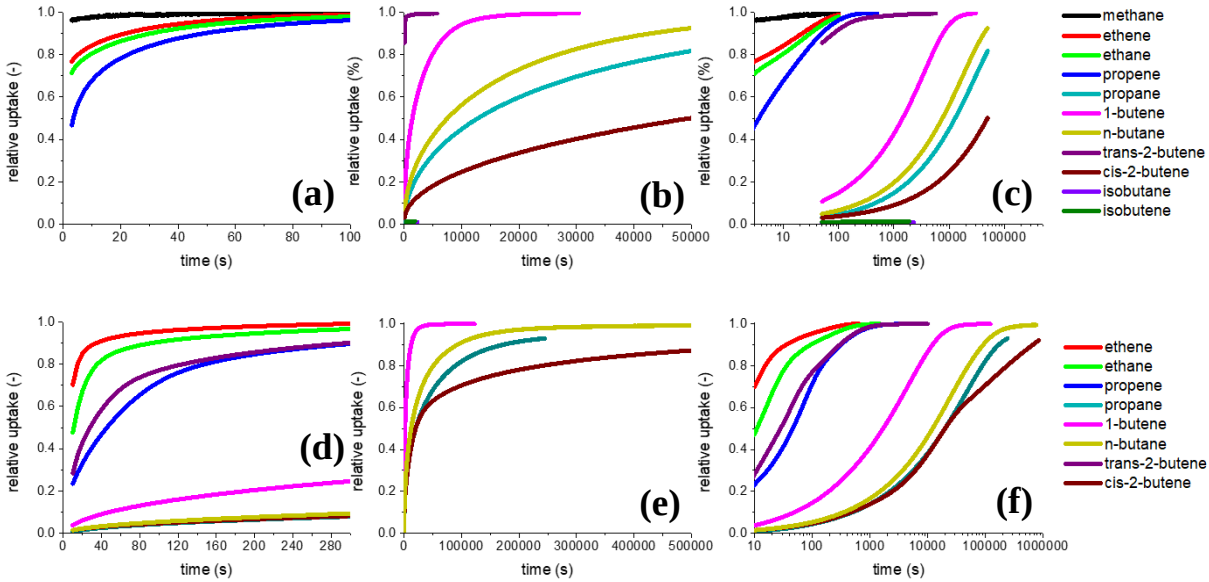

*Figure 20: The hydrocarbon uptake curves on the Si-**CHA** measured by volumetry (a-c), and by gravimetry (d-f).*

Very large differences in the uptake rates were observed among the tested gases. While methane was completely adsorbed already within a couple of seconds, ethane and ethene required hundreds of seconds to completely populate the pores of the sample. The most interesting results were obtained, however, for the generally much slower adsorption of the C_3 and C_4 hydrocarbons (see Table 3 for the values of diffusion coefficients estimated from the measured uptake curves by employing the simplified linear $\sqrt{t}$-law valid for low coverages[94], along with the computational results obtained by the developed methodology).

*Table 3: The summary of C_3 and C_4 hydrocarbon diffusivities on the Si-**CHA** material obtained from the gravimetric and volumetric uptake curves.*

gas	C_3H_6	C_3H_8	E-2-C_4H_8	Z-2-C_4H_8	1-C_4H_8	n-C_4H_{10}
D (m^2 s^{-1}) grav.	4.29×10^{-17}	1.37×10^{-19}	7.09×10^{-17}	1.16×10^{-19}	1.55×10^{-18}	1.93×10^{-19}
D (m^2 s^{-1}) vol.		1.72×10^{-19}		4.83×10^{-20}	1.61×10^{-18}	2.99×10^{-19}
D (m^2 s^{-1}) comp.	2.25×10^{-15}	4.97×10^{-18}	2.74×10^{-14}	5.27×10^{-22}	1.41×10^{-16}	6.52×10^{-18}

Particularly large uptake-rate differences were observed for propene and propane and for trans-2-butene and cis-2-butene respectively, which thus confirmed previously established findings described in the literature[52, 53, 93]. Generally speaking, the diffusion blocking of the C_3 and C_4 hydrocarbons increased in the following order: trans-2-butene ~ propene < 1-butene < n-butane < propane < cis-2-butene << isobutene ~ isobutane (both of which were found to be unable to diffuse into the channels). Despite the relatively large quantitative differences, this order was qualitatively in a perfect agreement with the computational predictions – the only differences being that in the volumetric experiments, propene seemed to diffuse faster than trans-2-butene, while in the gravimetric experiments, cis-2-butene had a very similar behavior to propane about until 30000 seconds has been reached, at which point their behavior clearly diverged. These slight disagreements for the 2-butene isomers may have been related to a minor presence of the other isomer in each of the gases (hydrocarbons of 99 % purity were used).

These results demonstrate the profound influence that the topology of a zeolite framework can exert on the adsorption of a set of otherwise very similar gas molecules. This influence, however, doesn't only have to consist of kinetically or sterically limiting the mass transport of some guest species while allowing others to diffuse through the pore openings. While the silicate framework is a chemically homogenous structure (characterized primarily by the

exposed oxygen atoms of a basic character), it has been observed that (chemically equivalent) pure-silica zeolite frameworks of different topologies exhibit clear differences in interaction energies when interacting with small gas molecules such as CO_2. While the CO_2 adsorption heat of the Si-**CHA** was measured to be about 24 kJ/mol (in line with the data from literature[77]), in the case of the related Si-**LTA** material the value is only about 20 kJ/mol[84], while for the Si-**MFI** zeolite (which possesses cylindrical pores composed of 10MR windows), the value reaches up to 26 kJ/mol[95]. Based on the nature of the channel systems of these three framework-types, it could be hypothesized that these differences are due to the different levels of "enclosure" of the CO_2 molecule by the adjacent channel walls. In the case of the Si-**LTA** material, the CO_2 molecule interacts largely with the relatively flat silicate walls of the very large cages; the Si-**MFI**, with its cylindrical pores, on the other hand, represents a much more confined space where the CO_2 molecule can interact with a larger section of the silicate framework. This would presumably maximize the non-specific dispersion interaction ($\phi_D + \phi_R$), which would lead to an increase in the adsorption heat by several kJ/mol.

To investigate the influence of the pore size (and thus the ability to confine a small guest molecule) on the adsorption of CO_2 (the main part of Aim 3 of the thesis), two germanosilicate materials (**UTL** and **UOV**) featuring large elliptic cylindrical channels (14 or 12MR), as well as a set of pure-silica materials obtained from these precursors through the ADOR process (see Section 5) featuring smaller pores of a similar shape, were acquired and subsequently tested. The adsorption isotherms of CO_2 measured on the studied materials are in the Fig. 21.

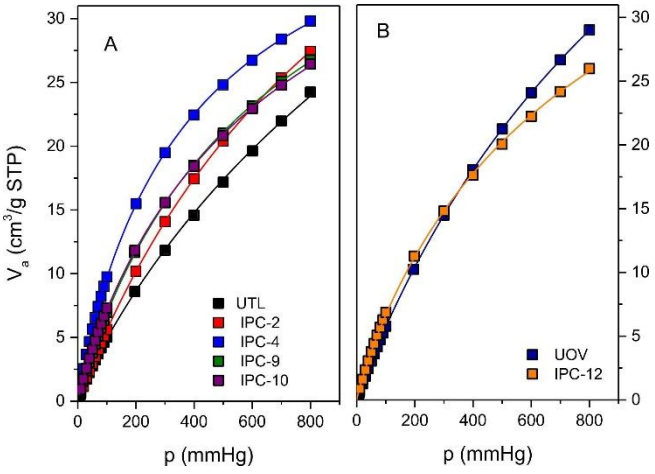

*Figure 21: Adsorption isotherms of the CO_2 on (A): parent **UTL** and **UTL**-derived IPC zeolites; (B) **UOV** and **UOV**-derived IPC-12 zeolite at 298 K.*

At low pressures (< 100 torr) a clear inverse correlation between the adsorption isotherm steepness and the pore size was observed, particularly in the case of the materials of the **UTL**

family (see Section 5, Fig. 9) – while for the **UTL** precursor itself (14 × 12MR) only about 5 cm^3/g STP CO_2 was adsorbed at 100 torr, for the IPC-2 (**OKO**) (12 × 10MR), IPC-10 (12 × 9MR) and IPC-4 (**PCR**) (10 × 8MR), it was about 6, 7.5 and 10 cm^3/g STP respectively. The IPC-9 material (10 × 7MR) exhibited a slightly lower uptake than expected (about 7.5 cm^3/g STP) which was likely related to the very low experimental micropore volume of the studied sample, possibly caused by insufficient material quality. The same general correlation between the low-pressure CO_2 uptakes and the pore size was also observed for the **UOV** and IPC-12 pair (see Section 5, Fig. 10). The observed differences were, however, comparably smaller, as the **UOV** family materials feature the 12 and 8MR channels perpendicularly passing through the layers. The presence of these large channels in both materials results in a smaller comparative difference in the nature of the **UOV** and IPC-12 channels when compared to the equivalent UTL and IPC-4 pair (where a 14 × 12MR channel system is fully transformed into a much narrower 10 × 8MR system), which explains the smaller difference in the adsorption isotherm steepness among the **UOV** and the IPC-12.

In order to gain further insight into the nature of the CO_2 interaction with the investigated zeolite frameworks, the isosteric adsorption heats were determined by the Clausius-Clapeyron equation (from a set of adsorption isotherms measured at multiple temperatures). The calculated values (see Fig. 22) once again very clearly correlate with the pore size of the zeolites. While the large-pore **UTL** exhibits a zero-coverage heat of about 23.5 kJ/mol (similar to the pure-silica **CHA** material, the 12 × 10MR IPC-2 (**OKO**) exhibits an adsorption heat of about 26 kJ/mol (similar to that of the 10MR pure-silica **MFI**). The remaining **UTL**-family materials with smaller pores exhibit even higher values of the CO_2 adsorption heat (the IPC-9 exhibited up to 33 kJ/mol).

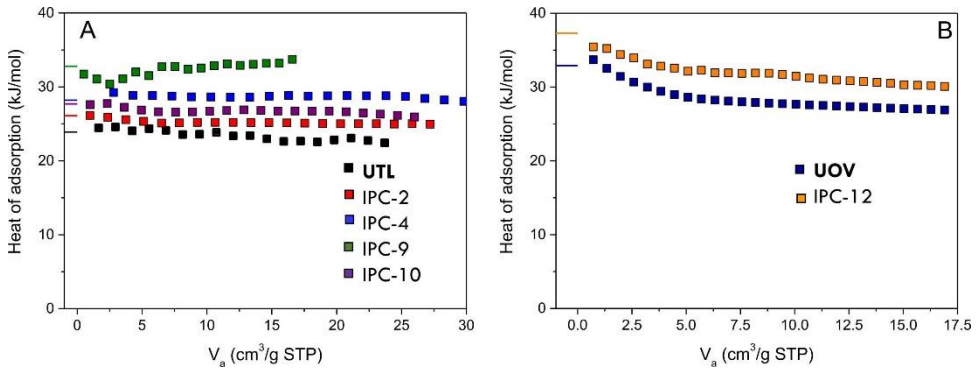

Figure 22: Isosteric heats of adsorption of CO_2 on the ADOR zeolites.

More interesting still is the case of the **UOV** and the IPC-12, both of which exhibit unexpectedly large zero-coverage CO_2 adsorption heats (33 and 37.3 kJ/mol, respectively), which, furthermore, clearly decrease with increasing uptake (by about 7 – 8 kJ/mol). This is in stark

contrast with the materials from the **UTL**-family, where the CO_2 adsorption heats remained largely constant with increasing uptakes. This behavior indicates that, unlike in the case of the **UTL**-family materials, the **UOV** and the IPC-12 materials contain channels with energetically very different positions vis-à-vis the CO_2 guest species, some of which seem to exhibit truly an exceptional affinity towards the CO_2.

To better understand the experimentally observed phenomena, the density functional theory/coupled cluster (DFT/CC) simulations at 300 K were performed by the collaborators from IOCB. The obtained results are generally in good agreement with the experimental observations (see Table 4 for the values of adsorption heats of the selected materials).

Table 4: Experimental and calculated adsorption heats of selected ADOR zeolites at zero coverages.

Parent	Material	ΔH_{CO_2} (exp.) (kJ/mol)	ΔH_{CO_2}(theor.) (kJ/mol)
UTL	IPC-2 (**OKO**)	26.1	22.8
	IPC-4 (**PCR**)	28.2	29.8
	IPC-9	32.8	29.4
	IPC-10	27.7	26.5
UOV	IPC-12	37.3	37.9

For the materials of the **UTL**-family, the computations systematically predict an increase in the interaction energy (consisting purely of the non-specific dispersive interactions - $\phi_D + \phi_R$) as the pore-size decreases (in the order of IPC-2 < IPC-10 < IPC-9 < IPC-4), which matches the experimental observations (with the exception of the IPC-9, where the experimentally obtained value is considerably higher than in the case of the IPC-4 – likely caused by the presence of a large quantity of hydroxyls due to the imperfect material quality). The presence of a more confined space doesn't, however, automatically imply the presence of a more stable binding site. This can be evidenced by the results on the IPC-4 (**PCR**) framework, which reveal that the most stable binding positions for the CO_2 guest molecule aren't located inside the 8MR channels, but rather inside the larger 10MR channels. Similarly, in the case of the IPC-10 material, the CO_2 molecule actually prefers a position at the entrance of the smaller 9MR window, where the molecule is protruding into the intersection with the larger 12MR channels (as opposed to the more confined positions in the middle of either of the channels).

Even more interesting, however, is the case of the IPC-12 material, where the exceptionally strong CO_2 binding has been attributed to the presence of a specific structural motif (illustrated

in Fig. 23a), which actually incorporates three different sub-motifs that have been previously discovered (computationally) to relatively strongly bind the CO_2 molecules[96].

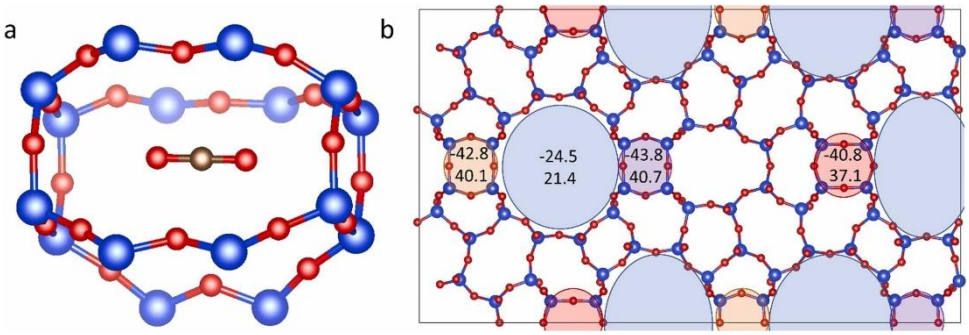

Figure 23: The CO_2 binding in IPC-12. (a) the binding motif, (b) the lowest interaction energy (negative) and the overall adsorption heat (positive) for a given space in IPC-12. Data from the 10 000 structures for which the DFT/CC energy is available (color code: Si blue, O red, C brown).

This binding motif for CO_2 in the IPC-12 zeolite comprises two 8MR windows (sufficiently large for the CO_2 transport not to be hindered, as verified by Force Field calculations), which are elongated in one direction and simultaneously narrowed in the other. Such an elongated small cage is then characterized by essentially the optimal size and shape to hold a CO_2 molecule, whose total interaction energy with the cage walls has been predicted to possibly reach over 40 kJ/mol (see Fig. 23b), a value comparable to the interaction energy of CO_2 with isolated K^+ EF cations localized in **CHA** zeolites, and higher than in the case of all the three alkali-metal forms of the **LTA**-4.5 material (see Table 2). It should be pointed out that the computational investigation further revealed that the interaction of the CO_2 molecule with this small cage doesn't consist only of non-specific interactions ($\phi_D + \phi_R$), but also contains a significant contribution from the interaction of the CO_2 quadrupole with the polar surface of the zeolite framework (ϕ_{FQ}), which explains the abnormally high adsorption heat.

While the presence of such highly specific motifs is very rare and is essentially impossible to tune (unlike the chemical composition or even possibly the framework dimensions – by for example the introduction of heteroatoms, see Section 7.1), the mechanism which leads to a highly selective interaction of selected molecules with specific elements of the channel system of a pure-silica zeolite could potentially find use in real processes, as it offers several major advantages – the very high affinity towards a specific molecule without the presence of a strong active site such as an EF cation would massively reduce problems with coking and adsorbent poisoning, furthermore the regeneration energy would likely be relatively low, nor would it be necessary to apply very long desorption times, which might be required to regenerate a kinetically selective adsorbent.

7.3. Preferred adsorption due to defects and impurities

While the adsorption preferences are usually driven by the regular features of the crystalline framework – whether it be the topology of the framework itself or its chemical nature (directly, or indirectly through the presence of EF cations and heteroatoms present in the framework) – in some systems, the discrimination between different types of molecules is driven by various irregular features present in the structure of the zeolite adsorbent. Arguably the most commonly exploited type of irregular site in zeolites are the silanol groups, which represent the simplest type of species which saturates defect sites in zeolites (generated, for example, by dealumination). The presence of these groups generally leads to an increase in the catalytic activity and hydrophilicity of the zeolite, leading to increases in uptakes of polar molecules. It can, however, also occasionally lead to reductions in mass transport of some molecules[97], which can be exploited for kinetically-driven separation processes. The relatively reactive defect sites can additionally be saturated by more complex species, such as some larger organic molecules. Such functionalized/grafted zeolite frameworks then exhibit various differences in properties compared to the unmodified frameworks, such as reduced pore volume and increased transport restrictions towards various gas molecules[98-100] – making it possible to employ the modified materials for specific kinetically-driven adsorption applications.

The presence of defect sites (or rather, of closely unidentified impurities that have reacted with the defect sites or block the channels) has been identified as the key driving force behind the observed separation effect in the last case study presented in this thesis, namely in the C_3 hydrocarbon adsorption on the **PCR** (IPC-4) zeolite synthesized by the ADOR process from the **UTL** precursor (whose investigation comprises the Aim 4 of the thesis). While the initial screening of the propane and propene adsorption (see Fig. 24) on the materials of the **UTL**-family generally revealed an ability of the materials to discriminate between propane and propene, the **PCR** (IPC-4) material exhibited nearly zero adsorption of propane in the whole studied pressure range (0 – 800 torr, at 303 K), completely overshadowing the performance of the other materials. This essentially absolute selectivity towards propene necessarily implied that both of the perpendicularly oriented 10MR and 8MR channels of the **PCR** framework had to be inaccessible for the propane molecules, while at least one of these channels remained largely accessible to propene. A similar, although less selective, phenomenon was likely observed in the case of the somewhat similar IPC-9 (containing a 10 × 7MR channel system) and IPC-10 (containing a 12 × 9MR channel system) frameworks, while in the case of the **OKO**

(IPC-2) framework, no selectivity was observed, as the channel system was likely fully accessible for both molecules.

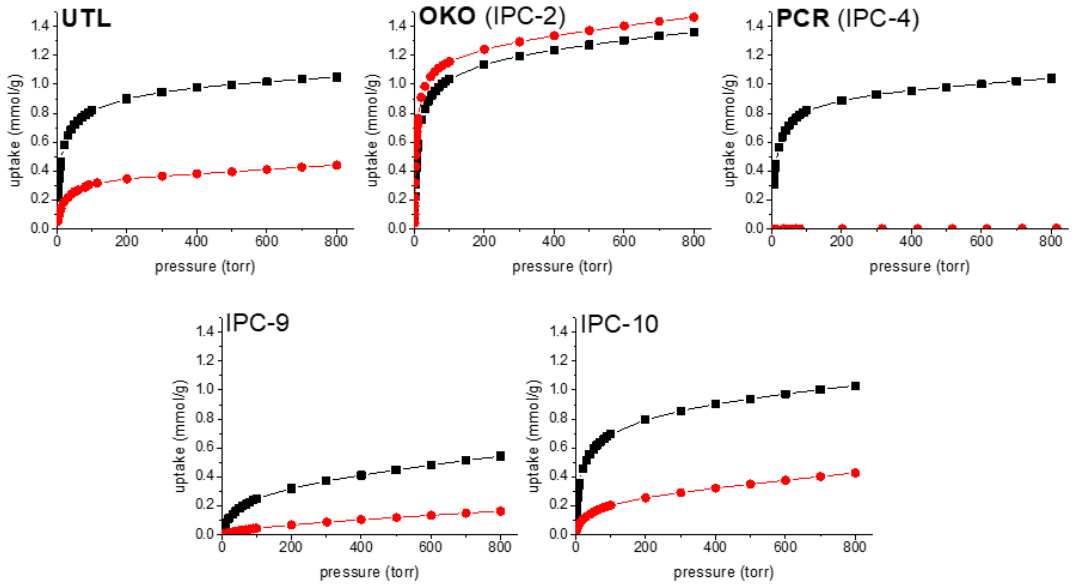

*Figure 24: The adsorption isotherms of propane (red) and propene (black) on the **UTL**-family ADOR zeolites (measured at 303 K)*

In order to verify the reproducibility of the very impressive results obtained on the **PCR** material, four further **PCR** batches (denoted as **PCR**-1, 2, 3, 4, while the sample shown above was denoted as **PCR**-0) were acquired and tested. While the adsorption measurements (see Fig. 25a for the C_3 hydrocarbon adsorption isotherms) confirmed the very clear preference of the framework towards the propene molecules, very large differences were nonetheless observed among all the investigated batches. Despite the fact that all the materials exhibited comparable values of the micropore volume (except for the **PCR**-4 material, whose micropore volume was by about 20 % larger than for the other materials), their propene uptakes differed significantly (ranging from about 0.5 mmol/g at 800 torr for the **PCR**-1 sample up to about 1.2 mmol/g for the **PCR**-3 sample).

Furthermore, none of the new batches exhibited such clear exclusion of propane from their channels as the **PCR**-0 material (the **PCR**-4 material even exhibited a somewhat sizeable adsorption of propane). The adsorption of propene and propane was additionally more closely investigated gravimetrically on the material **PCR**-3 (see Fig. 25b) (the best performing of the four samples), which revealed a ratio of diffusion coefficients of propene and propane of about 730. The results on these various batches strongly indicate that not only the transport of propane, but also the transport of propene is at least partially being restricted in the channels of the **PCR** framework.

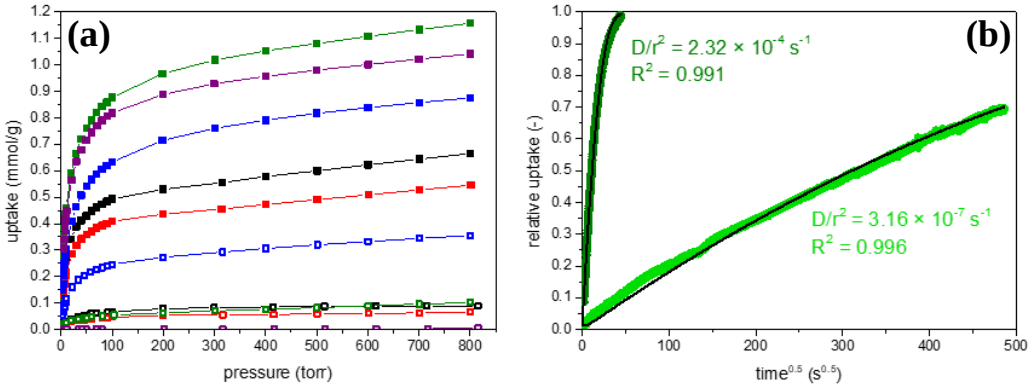

*Figure 25: (a) The adsorption isotherms of propene (■) and propane (□) at 303 K on **PCR**-0 (purple), **PCR**-1 (black), **PCR**-2 (red), **PCR**-3 (green) and **PCR**-4 (blue), (b) The propene (dark) and propane (light) uptake curves (at 303 K) on **PCR**-3.*

In order to obtain more insight into the nature of the hydrocarbon interaction with the **PCR** framework, molecular simulations were conducted by the collaborators from IOCB, investigating three possible modes of transport for both propene and propane – the diffusion along the main 10MR channel (m→m), the diffusion from the main 10MR channel into the 8MR side channel (m→s), and the diffusion from the 8MR side channel into the main 10MR channel (s→m). It was found that the narrower 8MR-windows should considerably hinder the transport of both propene and especially propane – the ratio of their diffusivities for the m→s and s→m modes of transport being approximately 140 and 1200 respectively, allowing for kinetics-based separation of the two hydrocarbon molecules. This result is generally in agreement with the experimentally observed diffusion coefficient ratio of about 730, calculated from the gravimetric uptake curves of the **PCR**-3 material. Interestingly enough, however, the simulations suggest, that the transport along the main 10MR channel (the m→m mode of transport) shouldn't be accompanied by any transport restrictions for either gas, which implies that the 10MR channels (and therefore the whole channel system) should be fully accessible for both molecules, in stark disagreement with the above presented experimental results. This result implies that the vast majority of the 10MR channels have to contain transport hindrances that partially or completely restrict the diffusion of hydrocarbon guest species, which are thus forced to bypass the obstacles through the smaller 8MR channels (perpendicular to the main 10MR channels) for the molecules to diffuse further into the crystal. Nonetheless, the 2-dimensional nature of the PCR channel system, whose pores run parallel along the sheet-like crystals, with openings strictly on the very narrow edges of the large flat crystals, suggests that a presence of only a relatively small number of species blocking the transport of guest molecules would suffice to bring about the required mass transport restriction and thus make the diffusion

through the 8MR windows the rate-determining step of the whole process. Such a mechanism would explain the experimentally observed adsorption behavior.

It has been hypothesized that these kinetic restrictions are due to the presence of foreign species and impurities present in the pores that were either intercalated between the layers during the synthesis (during the "disassembly" and "organization" steps) or bound to the very numerous defect sites brought about by an imperfect linking of the layers in the last step of the synthesis ("reassembly" step). The precise nature of these species is unknown, but the possibilities include either species containing Ge, such as extra-framework Ge^{4+} cations or GeO_2 deposits (residual Ge-content has been demonstrated by the chemical analysis – Si/Ge ranges from about 40 to 130) or alternatively some (likely amorphous) silica deposits.

The very high concentration of defects in the materials is evidenced by the high quantities of silanol groups in the PCR materials, as demonstrated by the in-situ FTIR spectra of the evacuated samples (after a treatment at 523 K) (see Fig. 26a).

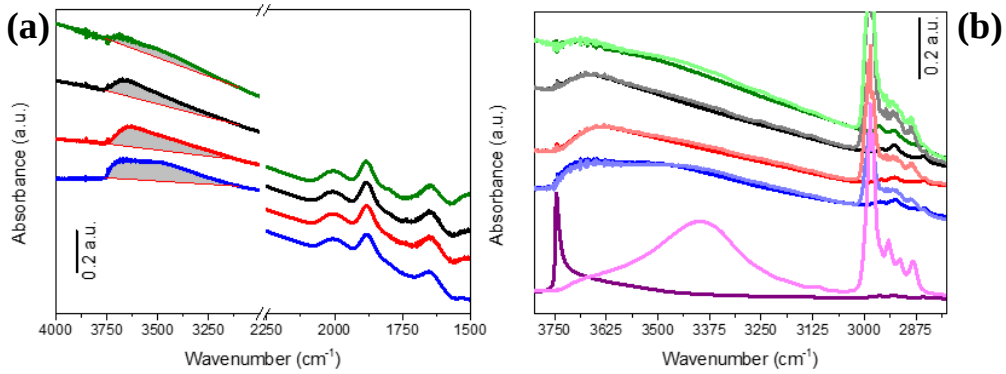

*Figure 26: The in-situ FTIR spectra of the evacuated (dark color) samples (a) and of the samples exposed to 6 torr of pivalonitrile (light color) for >15 minutes (b). The **PCR** spectra were normalized to the same Si-O overtone intensity. **PCR**-1 = black, **PCR**-2 = red, **PCR**-3 = green, **PCR**-4 = blue and the SBA-15 standard = purple.*

The spectra of the **PCR**-1, 2, 3, 4 materials reveal a presence of a very broad peak in the O–H vibration region (3750 – ~3200 cm^{-1}). Such a very broad signal is characteristic of a presence of predominantly variously partially or fully hydrogen-bonded O–H species in pure-silica zeolites and other materials[101-104]. The signal at 3745 cm^{-1} revealing the presence of fully isolated O–H groups can be seen for all four samples, but is very weak, indicating the near totality of the hydroxyl groups is present in arrangements where they interact with other hydroxyls or different species. The localization of the vast majority of the hydroxyl groups inside the pore system was confirmed by in-situ FTIR experiments employing the pivalonitrile (tert-butylnitrile) probe (see Fig. 26b), a Lewis base sufficiently large to not be able to diffuse into neither the 10MR or the 8MR channels. The exposition of the pre-treated material (at 523 K

for 90 minutes) to the probe led only to marginal changes in the O–H region, confirming the bulk of the hydroxyl species were located in the micropores inaccessible to the pivalonitrile probe (in contrast to a mesoporous silica standard SBA-15, where nearly all of the hydroxyls were found to interact with the probe).

The presence of the silanols and their localization largely inside the micropores of the material was further independently verified by ^{1}H spin-echo solid-state MAS NMR, employing a shift reagent d^{27}-[Eu(fod)$_3$], able to selectively mask selected signals of the NMR spectra.

Looking at the in-situ FTIR spectra of the evacuated samples (Fig. 26a), it should be pointed out that the most selective material (**PCR**-3) exhibits the lowest O-H band intensity, whereas the least selective material exhibits by far the highest O-H band intensity. It has been suggested that this inverse correlation is due to a differing occupancy of the defective sites inside the **PCR** structure (assumed to be present in comparable concentrations in all four samples) by the impurities and other foreign species restricting the hydrocarbon diffusion. As such, the very large quantity of hydroxyl groups present in the **PCR**-4 material indicates that only a comparably small fraction of the defects is occupied by other species that can exert influence on the transport of propane and propene, leading to a relatively low selectivity of the material. Meanwhile, in the case of the **PCR**-3 material, the relatively low concentration of the silanol groups can be explained by a relatively large occupancy of the defect sites by other species, which results in a much more significant restriction of especially propane diffusion, as upon entering the main 10MR channel, the hydrocarbon molecules are more frequently forced to bypass the obstructions by the perpendicularly oriented 8MR windows, through which propene diffuses by about 2 – 3 orders of magnitude faster (as shown by both the experiment – Fig. 25b and simulation).

It should be mentioned that a mechanism similar to the one proposed in this subsection might be able to explain some hitherto not completely understood behavior, such as the anomalously high olefin/paraffin selectivity of the pure-silica **RRO** (RUB-41) material[57, 105] (likewise obtained from a layered precursor), boasting considerably larger channels than the **PCR** material shown in this work, but nonetheless exhibiting a comparable selectivity.

8. CONCLUSIONS

Adsorptive separation employing zeolite adsorbents is an increasingly important method in a wide range of chemical, petroleum, and other large-scale industrial processes, particularly due to its capacity to replace the highly energy-intensive state-of-the-art distillation-based methods. As of now, a wider application of adsorption-based processes is limited by, among other things, the insufficient performance of established adsorbents, as well as by the lack of a sufficiently deep understanding of the underlying mechanism on the molecular scale. The implementation of more affordable capture and separation methods is particularly demanded in the field of CO_2 adsorption (due to the necessity to perform carbon capture, as well as the processing of various industrial gas mixtures containing other small molecules, such as CH_4, N_2, or CO) and in the field of hydrocarbon separation (particularly due to the exceedingly high costs of performing the fractionation of the olefin/paraffin mixtures).

This doctoral thesis set out to explore four specific research questions related to the successful application of zeolitic adsorbents (particularly of the **CHA** and **LTA** frameworks, as well as the hitherto uninvestigated materials synthesized by the recently developed ADOR procedure) in these two broad fields. These research questions included the investigation of the following phenomena: 1) the influence of different types of hetero-atoms on the CO_2/CH_4 adsorption on acidic **CHA** zeolites, 2) the localization of alkali-metal extra-framework cations and their influence on the CO_2/CH_4 adsorption on **CHA** and **LTA** zeolites, 3) the influence of the framework topology on both the CO_2, as well as light hydrocarbon adsorption on the **CHA** and ADOR-synthesized zeolites, and finally, 4) the anomalously high selectivity of one of the ADOR-synthesized materials – **PCR** – for propene/propane separation. The results obtained for each of the four research questions can be summarized as follows:

1) A clear influence of the heteroatom type (only Si, B, Al, Ga), present in the **CHA** framework, on the CO_2 and CH_4 adsorption was observed. The affinity of the materials towards CH_4 remained very similar, whereas their affinity towards CO_2 clearly increased in the order of Si-**CHA** < B-**CHA** < Ga-**CHA** < Al-**CHA**, as evidenced both by the adsorbed amounts, as well as the values of the CO_2 interaction energy, which nonetheless increased only modestly – making Al-**CHA** the best performing material. These changes in affinity were primarily ascribed to the changes in the acidity of the active sites present in the respective materials, although they may have also been connected to changes in the framework geometry (as evidenced by the PXRD experiments).

2) Clearly different localization preferences inside the **CHA** pore system were observed for each of the three alkali-metal cations (Li^+, Na^+, K^+), particularly with changing Si/Al. While the higher-silica frameworks (Si/Al > 8) exhibit the previously reported preferences (Li^+, Na^+ prefer the 6MR, K^+ prefers the 8MR pore entrance), the frameworks with Si/Al ≈ 2 exhibit significantly altered site occupancies (e.g., large occupancy of the 8MR pore entrance even by the Na^+ cations), resulting in observable influence on the CO diffusion into the channel system. The comprehensive investigation of CO_2/CH_4 adsorption on the high/medium-silica **CHA** and **LTA** (Si/Al = 4.5) revealed a complex influence of the cation type on the adsorbent performance, manifesting itself differently for both the **CHA** and **LTA** frameworks. Of the studied materials, the **LTA** frameworks exhibited the best CO_2/CH_4 separation performance (the identification of which cationic form is optimal would require tests under real industrial conditions).

3) Both the pore size, as well as the pore shape, were identified as key factors influencing the CO_2 adsorption on the electroneutral frameworks derived from the **UTL** and **UOV** precursors by the ADOR process. Smaller channel width was found to generally result in a stronger CO_2 adsorption, albeit the CO_2 wasn't always necessarily located in the most confined parts of the channel system. The **UOV**-derived IPC-12 material was found to exhibit an exceptional affinity towards CO_2 due to the presence of characteristic structural motifs capable of strongly encapsulating the CO_2 molecules. The **UTL**-derived materials, furthermore, exhibited various capacities to adsorb propane and propene – the propene/propane selectivity increased as the pore size decreased, with the small pore **PCR** material capable of clearly the largest separation effect.

4) Repeated propene/propane adsorption experiments on additional **PCR** batches revealed that the observed effect was only partially reproducible – each batch was found to be clearly selective towards propene, but to differing extents. Computational investigation was further found to be unable to predict the observed behavior. A possible interpretation, which would explain the experimental observations in light of the computational results, was developed – assuming the presence of obstructing impurities in the **PCR** channels, rendering the diffusion through the smaller 8MR pores the rate-determining step. The likely presence of these foreign species was indirectly demonstrated by the use of advanced in-situ FTIR and MAS NMR experiments.

REFERENCES

(1) R.T. Jacobsen, et al., Thermodynamic Properties of Nitrogen from the Freezing Line to 2000 K at Pressures to 1000 MPa, Journal of Physical and Chemical Reference Data, 15 (1986) 735-909. DOI: 10.1063/1.555754.
(2) W. Pentermann, et al., New pressure-density-temperature measurements and new rational equations for the saturated liquid and vapour densities of oxygen, The Journal of Chemical Thermodynamics, 10 (1978) 1161-1172. DOI: 10.1016/0021-9614(78)90033-2.
(3) A. Van Miltenburg, et al., Adsorptive Separation of Light Olefin/Paraffin Mixtures, Chemical Engineering Research and Design, 84 (2006) 350-354. DOI: 10.1205/cherd05021.
(4) C.M. Yon, et al., Adsorption, Gas Separation, in: Kirk-Othmer Encyclopedia of Chemical Technology, 2003, ISBN: 9780471238966.
(5) https://goldbook.iupac.org/terms/view/A00155, Accessed November 4th, 2024.
(6) J. James, et al., Review of technologies for carbon monoxide recovery from nitrogen-containing industrial streams, Frontiers in Chemical Engineering, 5 (2023) DOI: 10.3389/fceng.2023.1066091.
(7) R.T. Yang, Adsorbents: Fundamentals and Applications, ed., Wiley, 2003. ISBN: 9780471297413.
(8) T. Sen, et al., Integration of Material and Process Design for Kinetic Adsorption Separation, Industrial & Engineering Chemistry Research, 60 (2021) 2536-2546. DOI: 10.1021/acs.iecr.0c05138.
(9) M. Alhamami, et al., A Review on Breathing Behaviors of Metal-Organic-Frameworks (MOFs) for Gas Adsorption, Materials (Basel), 7 (2014) 3198-3250. DOI: 10.3390/ma7043198.
(10) L. Li, et al., Discrimination of xylene isomers in a stacked coordination polymer, Science, 377 (2022) 335-339. DOI: 10.1126/science.abj7659.
(11) P.J. Bereciartua, et al., Control of zeolite framework flexibility and pore topology for separation of ethane and ethylene, Science, 358 (2017) 1068-1071. DOI: 10.1126/science.aao0092.
(12) J. Shang, et al., Discriminative Separation of Gases by a "Molecular Trapdoor" Mechanism in Chabazite Zeolites, Journal of the American Chemical Society, 134 (2012) 19246-19253. DOI: 10.1021/ja309274y.
(13) J. Shang, et al., Separation of CO2 and CH4 by Pressure Swing Adsorption Using a Molecular Trapdoor Chabazite Adsorbent for Natural Gas Purification, Industrial & Engineering Chemistry Research, 59 (2020) 7857-7865. DOI: 10.1021/acs.iecr.0c00317.
(14) A.F. Cronstedt, Rön och beskrifning om en obekant bärg art, som kallas zeolites, Kungliga Svenska Vetenskapsakademiens Handlingar, 17 (1756) 120-123.
(15) D.S. Coombs, et al., Recommended nomenclature for zeolite minerals: report of the subcommittee on zeolites of the International Mineralogical Association, Commission on New Minerals and Mineral Names, Mineralogical Magazine, 62 (1998) 533-571. DOI: 10.1180/002646198547800.
(16) L.B. McCusker, et al., Nomenclature of structural and compositional characteristics of ordered microporous and mesoporous materials with inorganic hosts (IUPAC Recommendations 2001), 73 (2001) 381-394. DOI: 10.1351/pac200173020381.
(17) W. Loewenstein, The distribution of aluminum in the tetrahedra of silicates and aluminates, American Mineralogist, 39 (1954) 92-96.
(18) P. Baile, et al., Zeolites and zeolite-based materials in extraction and microextraction techniques, Analyst, 144 (2019) 366-387. DOI: 10.1039/C8AN01194J.
(19) C. Klein, et al., Earth Materials: Introduction to Mineralogy and Petrology, 2 ed., Cambridge University Press, Cambridge, 2016. ISBN: 9781316608852.

(20) Z. Asgar Pour, et al., A Review on the Effects of Organic Structure-Directing Agents on the Hydrothermal Synthesis and Physicochemical Properties of Zeolites, Chemistry, 4 (2022) 431-446. DOI: 10.3390/chemistry4020032.
(21) X. Li, et al., Why Zeolites Have So Few Seven-Membered Rings, The Journal of Physical Chemistry C, 118 (2014) 15835-15839. DOI: 10.1021/jp504143r.
(22) R. Pophale, et al., A database of new zeolite-like materials, Physical Chemistry Chemical Physics, 13 (2011) 12407-12412. DOI: 10.1039/C0CP02255A.
(23) A. Erlebach, et al., Accurate large-scale simulations of siliceous zeolites by neural network potentials, npj Computational Materials, 8 (2022) 174. DOI: 10.1038/s41524-022-00865-w.
(24) https://europe.iza-structure.org/IZA-SC/ftc_table.php, Accessed May 26th, 2025.
(25) https://europe.iza-structure.org/IZA-SC/SBUList.html, Accessed May 26th, 2025.
(26) C. Baerlocher, et al., Introduction and explanatory notes, in: C. Baerlocher, L.B. McCusker, D.H. Olson (Eds.) Atlas of Zeolite Framework Types (Sixth Edition), Elsevier Science B.V., Amsterdam, 2007, pp. 3-11. ISBN: 9780444530646.
(27) N.A. Anurova, et al., Natural Tilings for Zeolite-Type Frameworks, The Journal of Physical Chemistry C, 114 (2010) 10160-10170. DOI: 10.1021/jp1030027.
(28) V.A. Blatov, et al., Three-periodic nets and tilings: natural tilings for nets, Acta Crystallogr A, 63 (2007) 418-425. DOI: 10.1107/s0108767307038287.
(29) H.K. Beyer, Dealumination Techniques for Zeolites, in: Post-Synthesis Modification I, Springer Berlin Heidelberg, Berlin, Heidelberg, 2002, pp. 203-255. ISBN: 978-3-540-69750-3.
(30) S. Ghojavand, et al., Flexibility in zeolites: origin, limits, and evaluation, Chemical Science, 14 (2023) 12430-12446. DOI: 10.1039/D3SC03934J.
(31) B. Ilić, et al., A review of adsorbate and temperature-induced zeolite framework flexibility, Microporous and Mesoporous Materials, 239 (2017) 221-234. DOI: 10.1016/j.micromeso.2016.10.005.
(32) D.R. Corbin, et al., Flexibility of the zeolite RHO framework: in situ x-ray and neutron powder structural characterization of divalent cation-exchanged zeolite RHO, Journal of the American Chemical Society, 112 (1990) 4821-4830. DOI: 10.1021/ja00168a029.
(33) T.M. Nenoff, et al., Flexibility of the Zeolite RHO Framework. In Situ X-ray and Neutron Powder Structural Characterization of Cation-Exchanged BePO and BeAsO RHO Analogs, The Journal of Physical Chemistry, 100 (1996) 14256-14264. DOI: 10.1021/jp9604296.
(34) B. Ma, et al., Thermodynamic study of cement/rock interactions using experimentally generated solubility data of zeolites, Cement and Concrete Research, 135 (2020) 106149. DOI: 10.1016/j.cemconres.2020.106149.
(35) S. Davis, et al., CEH marketing research report: zeolites, SRI Consulting, 599 (2009).
(36) M. Mazur, et al., Zeolites and Other Micro- and Mesoporous Molecular Sieves, in: Kirk-Othmer Encyclopedia of Chemical Technology, 2019, pp. 1-36. ISBN: 9780471238966.
(37) R.W. Broach, et al., Zeolites, in: Ullmann's Encyclopedia of Industrial Chemistry, 2012, ISBN: 9783527306732.
(38) D.G. Boer, et al., Zeolites as Selective Adsorbents for CO2 Separation, ACS Applied Energy Materials, 6 (2023) 2634-2656. DOI: 10.1021/acsaem.2c03605.
(39) D. Bonenfant, et al., Advances in principal factors influencing carbon dioxide adsorption on zeolites, Science and Technology of Advanced Materials, 9 (2008) 013007. DOI: 10.1088/1468-6996/9/1/013007.
(40) K.C. Kemp, et al., Small Gas Adsorption and Separation in Small-Pore Zeolites, in: S. Valencia, F. Rey (Eds.) New Developments in Adsorption/Separation of Small Molecules by Zeolites, Springer International Publishing, Cham, 2020, pp. 1-30. ISBN: 978-3-030-63853-5.
(41) R. Bai, et al., Low-energy adsorptive separation by zeolites, National Science Review, 9 (2022) nwac064. DOI: 10.1093/nsr/nwac064.

(42) R.-S. Liu, et al., Advances in Post-Combustion CO2 Capture by Physical Adsorption: From Materials Innovation to Separation Practice, ChemSusChem, 14 (2021) 1428-1471. DOI: 10.1002/cssc.202002677.
(43) S. Kumar, et al., Utilization of zeolites as CO2 capturing agents: Advances and future perspectives, Journal of CO2 Utilization, 41 (2020) 101251. DOI: 10.1016/j.jcou.2020.101251.
(44) D. Fu, et al., Carbon dioxide capture with zeotype materials, Chemical Society Reviews, 51 (2022) 9340-9370. DOI: 10.1039/D2CS00508E.
(45) E. Pérez-Botella, et al., Zeolites in Adsorption Processes: State of the Art and Future Prospects, Chemical Reviews, 122 (2022) 17647-17695. DOI: 10.1021/acs.chemrev.2c00140.
(46) Y. Wang, et al., Alternatives to Cryogenic Distillation: Advanced Porous Materials in Adsorptive Light Olefin/Paraffin Separations, Small, 15 (2019) 1900058. DOI: 10.1002/smll.201900058.
(47) M. Gehre, et al., Sustainable Separations of C4-Hydrocarbons by Using Microporous Materials, ChemSusChem, 10 (2017) 3947-3963. DOI: 10.1002/cssc.201700657.
(48) A. Burton, Recent trends in the synthesis of high-silica zeolites, Catalysis Reviews, 60 (2018) 132-175. DOI: 10.1080/01614940.2017.1389112.
(49) P. Eliášová, et al., The ADOR mechanism for the synthesis of new zeolites, Chemical Society Reviews, 44 (2015) 7177-7206. DOI: 10.1039/C5CS00045A.
(50) S. Mintova, et al., Nanosized zeolites: Quo Vadis?, Comptes Rendus. Chimie, 19 (2016) 183-191. DOI: 10.1016/j.crci.2015.11.005.
(51) A. Kuperman, et al., Non-aqueous synthesis of giant crystals of zeolites and molecular sieves, Nature, 365 (1993) 239-242. DOI: 10.1038/365239a0.
(52) D.H. Olson, Light hydrocarbon separation using 8-member ring zeolites, US6488741B2 (2002).
(53) D.H. Olson, et al., Light hydrocarbon sorption properties of pure silica Si-CHA and ITQ-3 and high silica ZSM-58, Microporous and Mesoporous Materials, 67 (2004) 27-33. DOI: 10.1016/j.micromeso.2003.09.025.
(54) S.C. Reyes, et al., Separation of propylene from hydrocarbon mixtures, US6730142B2 (2004).
(55) J. Gascon, et al., Accelerated synthesis of all-silica DD3R and its performance in the separation of propylene/propane mixtures, Microporous and Mesoporous Materials, 115 (2008) 585-593. DOI: 10.1016/j.micromeso.2008.02.038.
(56) M. Palomino, et al., Pure silica ITQ-32 zeolite allows separation of linear olefins from paraffins, Chemical Communications, (2007) 1233-1235. DOI: 10.1039/B700358G.
(57) T.D. Pham, et al., Adsorption equilibria of CO2 and small hydrocarbons in AEI-, CHA-, STT-, and RRO-type siliceous zeolites, Microporous and Mesoporous Materials, 236 (2016) 100-108. DOI: 10.1016/j.micromeso.2016.08.025.
(58) Q. Yue, et al., Seeded growth of isomorphously substituted chabazites in proton-form, Microporous and Mesoporous Materials, 280 (2019) 331-336. DOI: 10.1016/j.micromeso.2019.02.017.
(59) B.E. Poling, et al., Properties of Gases and Liquids, 5th ed., McGraw-Hill Education, New York, 2001. ISBN: 9780070116825.
(60) https://cccbdb.nist.gov/diplistx.asp, Accessed May 23rd, 2025.
(61) https://cccbdb.nist.gov/quadlistx.asp, Accessed May 23rd, 2025.
(62) https://cccbdb.nist.gov/pollistx.asp, Accessed May 23rd, 2025.
(63) E.M. Flanigen, et al., Aluminophosphate Molecular Sieves and the Periodic Table, in: Y. Murakami, A. Iijima, J.W. Ward (Eds.) Studies in Surface Science and Catalysis, Elsevier, 1986, pp. 103-112. ISBN: 0167-2991.
(64) D.R. Peacor, et al., Willhendersonite, a new zeolite isostructural with chabazite, American Mineralogist, 69 (1984) 186-189.

(65) W.J. Roth, et al., A family of zeolites with controlled pore size prepared using a top-down method, Nat Chem, 5 (2013) 628-633. DOI: 10.1038/nchem.1662.
(66) P.S. Wheatley, et al., Zeolites with Continuously Tuneable Porosity, Angewandte Chemie International Edition, 53 (2014) 13210-13214. DOI: 10.1002/anie.201407676.
(67) E. Verheyen, et al., Design of zeolite by inverse sigma transformation, Nature Materials, 11 (2012) 1059-1064. DOI: 10.1038/nmat3455.
(68) S.E. Henkelis, et al., A procedure for identifying possible products in the assembly–disassembly–organization–reassembly (ADOR) synthesis of zeolites, Nature Protocols, 14 (2019) 781-794. DOI: 10.1038/s41596-018-0114-6.
(69) J.-L. Paillaud, et al., Extra-Large-Pore Zeolites with Two-Dimensional Channels Formed by 14 and 12 Rings, Science, 304 (2004) 990-992. DOI: 10.1126/science.1098242.
(70) Y. Lorgouilloux, et al., IM-17: a new zeolitic material, synthesis and structure elucidation from electron diffraction ADT data and Rietveld analysis, RSC Advances, 4 (2014) 19440-19449. DOI: 10.1039/C4RA01383B.
(71) R. Castañeda, et al., Synthesis of a New Zeolite Structure ITQ-24, with Intersecting 10- and 12-Membered Ring Pores, Journal of the American Chemical Society, 125 (2003) 7820-7821. DOI: 10.1021/ja035534p.
(72) A. Corma, et al., A zeolite with interconnected 8-, 10- and 12-ring pores and its unique catalytic selectivity, Nature Materials, 2 (2003) 493-497. DOI: 10.1038/nmat921.
(73) M. Mazur, et al., Synthesis of 'unfeasible' zeolites, Nat Chem, 8 (2016) 58-62. DOI: 10.1038/nchem.2374.
(74) O. Veselý, et al., Reverse ADOR: reconstruction of UTL zeolite from layered IPC-1P, Materials Advances, 2 (2021) 3862-3870. DOI: 10.1039/D1MA00212K.
(75) V. Kasneryk, et al., Insight into the ADOR zeolite-to-zeolite transformation: the UOV case, Dalton Transactions, 47 (2018) 3084-3092. DOI: 10.1039/C7DT03751A.
(76) V. Kasneryk, et al., Expansion of the ADOR Strategy for the Synthesis of Zeolites: The Synthesis of IPC-12 from Zeolite UOV, Angewandte Chemie International Edition, 56 (2017) 4324-4327. DOI: 10.1002/anie.201700590.
(77) T.D. Pham, et al., Molecular Basis for the High CO2 Adsorption Capacity of Chabazite Zeolites, ChemSusChem, 7 (2014) 3031-3038. DOI: 10.1002/cssc.201402555.
(78) M.R. Hudson, et al., Unconventional, Highly Selective CO2 Adsorption in Zeolite SSZ-13, Journal of the American Chemical Society, 134 (2012) 1970-1973. DOI: 10.1021/ja210580b.
(79) A.C. Safont, et al., Brønsted acidity of H-[Ga]-ZSM-5 zeolites as determined by variable-temperature IR spectroscopy, Catalysis Today, 345 (2020) 71-79. DOI: 10.1016/j.cattod.2019.10.015.
(80) A. Pulido, et al., Combined DFT/CC and IR spectroscopic studies on carbon dioxide adsorption on the zeolite H-FER, Energy & Environmental Science, 2 (2009) 1187-1195. DOI: 10.1039/B911253G.
(81) M.R. Delgado, et al., Carbon monoxide, dinitrogen and carbon dioxide adsorption on zeolite H-Beta: IR spectroscopic and thermodynamic studies, Energy, 36 (2011) 5286-5291. DOI: 10.1016/j.energy.2011.06.033.
(82) B. Bonelli, et al., Experimental and Quantum Chemical Studies on the Adsorption of Carbon Dioxide on Alkali-Metal-Exchanged ZSM-5 Zeolites, The Journal of Physical Chemistry B, 104 (2000) 10978-10988. DOI: 10.1021/jp000555g.
(83) S.-J. Hwang, et al., Boron Sites in Borosilicate Zeolites at Various Stages of Hydration Studied by Solid State NMR Spectroscopy, The Journal of Physical Chemistry B, 108 (2004) 18535-18546. DOI: 10.1021/jp0476904.

(84) A.S. Hyla, et al., Significant Temperature Dependence of the Isosteric Heats of Adsorption of Gases in Zeolites Demonstrated by Experiments and Molecular Simulations, The Journal of Physical Chemistry C, 123 (2019) 20405-20412. DOI: 10.1021/acs.jpcc.9b05758.
(85) M. Palomino, et al., New Insights on CO2−Methane Separation Using LTA Zeolites with Different Si/Al Ratios and a First Comparison with MOFs, Langmuir, 26 (2010) 1910-1917. DOI: 10.1021/la9026656.
(86) G.D. Pirngruber, et al., The role of the extra-framework cations in the adsorption of CO2 on faujasite Y, Physical Chemistry Chemical Physics, 12 (2010) 13534-13546. DOI: 10.1039/B927476F.
(87) H.V. Thang, et al., Adsorption of CO2 in FAU zeolites: Effect of zeolite composition, Catalysis Today, 227 (2014) 50-56. DOI: 10.1016/j.cattod.2013.10.036.
(88) R. Bulánek, et al., Microcalorimetric and FTIR Study of the Adsorption of Carbon Dioxide on Alkali-Metal Exchanged FER Zeolites, Topics in Catalysis, 53 (2010) 1349-1360. DOI: 10.1007/s11244-010-9593-6.
(89) W.J. Mortier, et al., Positions of cations and molecules in zeolites with the chabazite framework III. Dehydrated Na-exchanged chabazite, Materials Research Bulletin, 12 (1977) 241-249. DOI: 10.1016/0025-5408(77)90141-6.
(90) A. Alberti, et al., Position of cations and water molecules in hydrated chabazite. Natural and Na-, Ca-, Sr- and K-exchanged chabazites, Zeolites, 2 (1982) 303-309. DOI: 10.1016/S0144-2449(82)80075-4.
(91) P. Ugliengo, et al., Carbon monoxide adsorption on alkali and proton-exchanged chabazite: an ab-initio periodic study using the CRYSTAL code, Molecular Physics, 103 (2005) 2559-2571. DOI: 10.1080/00268970500180865.
(92) P.A. Barrett, et al., ITQ-12: a new microporous silica polymorph potentially useful for light hydrocarbon separations, Chemical Communications, (2003) 2114-2115. DOI: 10.1039/B306440A.
(93) G.L. Casty, et al., Separation of 1-butene from C4 feed streams, US2004/0260138A1 (2004).
(94) J. Kärger, et al., Diffusion in nanoporous materials with special consideration of the measurement of determining parameters (IUPAC Technical Report), 97 (2025) 1-89. DOI: 10.1515/pac-2023-1126.
(95) J.A. Dunne, et al., Calorimetric Heats of Adsorption and Adsorption Isotherms. 1. O2, N2, Ar, CO2, CH4, C2H6, and SF6 on Silicalite, Langmuir, 12 (1996) 5888-5895. DOI: 10.1021/la960495z.
(96) R.L. Martin, et al., Similarity-Driven Discovery of Zeolite Materials for Adsorption-Based Separations, ChemPhysChem, 13 (2012) 3595-3597. DOI: 10.1002/cphc.201200554.
(97) I.C. Medeiros-Costa, et al., Silanol defect engineering and healing in zeolites: opportunities to fine-tune their properties and performances, Chemical Society Reviews, 50 (2021) 11156-11179. DOI: 10.1039/D1CS00395J.
(98) V. Tejavath, et al., Technoeconomic Investigation of Amine-Grafted Zeolites and Their Kinetics for CO2 Capture, ACS Omega, 6 (2021) 6153-6162. DOI: 10.1021/acsomega.0c05397.
(99) C. Chen, et al., CO2 capture by amine-functionalized nanoporous materials: A review, Korean Journal of Chemical Engineering, 31 (2014) 1919-1934. DOI: 10.1007/s11814-014-0257-2.
(100) D. Kwon, et al., Tailoring the CO2 selective adsorption properties of MOR zeolites by post functionalization, Journal of CO2 Utilization, 62 (2022) 102064. DOI: 10.1016/j.jcou.2022.102064.

(101) A. Zecchina, et al., Silicalite characterization. 1. Structure, adsorptive capacity, and IR spectroscopy of the framework and hydroxyl modes, The Journal of Physical Chemistry, 96 (1992) 4985-4990. DOI: 10.1021/j100191a047.
(102) A. Zecchina, et al., Silicalite characterization. 2. IR spectroscopy of the interaction of carbon monoxide with internal and external hydroxyl groups, The Journal of Physical Chemistry, 96 (1992) 4991-4997. DOI: 10.1021/j100191a048.
(103) R.S. McDonald, Surface Functionality of Amorphous Silica by Infrared Spectroscopy, The Journal of Physical Chemistry, 62 (1958) 1168-1178. DOI: 10.1021/j150568a004.
(104) A. Burneau, et al., Comparative study of the surface hydroxyl groups of fumed and precipitated silicas. 2. Characterization by infrared spectroscopy of the interactions with water, Langmuir, 6 (1990) 1364-1372. DOI: 10.1021/la00098a008.
(105) Y.X. Wang, et al., Synthesis and Crystal Structure of Zeolite RUB-41 Obtained as Calcination Product of a Layered Precursor: a Systematic Approach to a New Synthesis Route, Chemistry of Materials, 17 (2005) 43-49. DOI: 10.1021/cm048677z.